PASSIVE DRAG SAIL APPLICATIONS FOR THE ACCELERATED DEORBIT AND TARGETED REENTRY OF SPACECRAFT

by

ANDREW MICHAEL SWEETEN

ROHAN SOOD, COMMITTEE CHAIR
DEAN M. TOWNSLEY
JOHN G. BAKER

A THESIS

Submitted in partial fulfillment of the requirements
for the degree of Master of Science in the
Department of Aerospace Engineering
and Mechanics in the Graduate
School of The University
of Alabama

TUSCALOOSA, ALABAMA

2021

ABSTRACT

In the relatively short time that space has been an asset to humans, the amount of debris occupying the region has become a noticeable concern. Maintaining the usability of space for future generations requires consideration of novel methods to remove debris and otherwise prevent space from becoming further congested. One such proposed method is aerodynamic drag sails to accelerate the natural deorbit process caused by the high-altitude atmosphere. The method, properly implemented, could cause the spacecraft to reenter the atmosphere and burn up without requiring the planning of additional maneuvers, potentially saving time and money while still meeting international requirements. Analysis of the technique requires solving the expected times in orbit and selecting a sail that optimizes cost relative to the spacecraft's orbital lifetime, initially using CubeSats. Atmospheric drag, however, is only one of many forces that may perturb a spacecraft along its trajectory. Solar radiation pressure is another source of perturbing forces acting on large surfaces in the direction of the Sun. After including these forces in high-fidelity deorbit analysis, one can predict where the spacecraft would likely impact the Earth if components do not burn up in Earth's atmosphere. To prioritize the safety of life and property on the surface, legal requirements dictate the location where the spacecraft may impact the surface. Since a passive drag sail does not have active control authority, the sail's initial deployment timing, orientation, and altitude dictate the final reentry point for a given gravitational and atmospheric drag model. Based on specific initial conditions, it is possible to show that a drag sail is an effective and efficient method of safely deorbiting a spacecraft while optimizing cost and conforming to legal requirements.

LIST OF ABBREVIATIONS AND SYMBOLS

A	Exposed Frontal Area
a	Semi-Major Axis
$a_{2,4}$	Coefficients for Geodetic Conversion
α	Sun Vector Angle of Attack
AU	Astronomical Unit
c	Speed of Light
C_d	Drag Coefficient
C_r	Radiation Pressure Coefficient
D	Drag Force
e	Eccentricity
$\hat{e}$	Eccentricity of Earth Spheroid
ε	Obliquity
F_N	Radiation Force
g	Gravitational Acceleration
h	Angular Momentum
h_e	Effective Altitude
h_p	Perigee Altitude
I_{sp}	Specific Impulse
i	Inclination
J_0	Solar Constant

J_2	J2 Perturbation Constant
JD	Julian Date
K_{SRP}	Solar Radiation Pressure Constant
L	Mean Longitude of the Sun
λ	Solar Ecliptic Longitude
λ_E	Earth Longitude
M	Mean Anomaly of the Sun
m	Spacecraft Mass
n	Days since J2000
Ω	Right Ascension of the Ascending Node
θ	True Anomaly
Φ	Latitude
φ	Flight Path Angle
P	Period
p	Perturbing Force
ρ	Atmospheric Density
r	Orbital Radius
RA	Right Ascension
s	Spacecraft Side Length
SR	Sun Unit Vector
t	Time
u	Argument of Latitude
μ	Gravitational Parameter

v	Velocity
ν	Shadow Function
ω	Argument of Perigee
$\hat{\omega}$	Earth Rotation Rate
x,y,z	Cartesian Position Coordinates

ACKNOWLEDGEMENTS

With the next phase of my education coming to a close, I would first and foremost like to thank my family for being there every step of the way. Thank you for instilling in me the importance of education and the drive to push further toward success. I could not have made it this far without the love and support you have given me through many long years of study. Thank you for believing in me even in times when I did not even believe in myself.

Next, I would like to thank the faculty and staff at the University of Alabama for providing the knowledge and means to pursue my education further. Thank you to Dr. Rohan Sood, my advisor, for helping guide me through the new and unique challenges of academic research. Thank you for constantly pushing me to be better and providing invaluable guidance through my endeavors. Also, thank you to Dr. Baker and Dr. Townsley for taking valuable time out of your schedules to review and provide feedback on my work.

Thank you to the other students in the Astrodynamics and Space Research Laboratory for giving me a place to feel welcome at the university. You all motivated me to continue striving and exemplified the type of student I wish I could be. Thank you for all the assistance and support throughout classes and research.

I would finally like to thank my closest friends from back in San Diego, affectionately known as the Dank Squad. I would never have made it through my undergraduate program, let alone to here, without everything I learned with and from you guys. Thank you for all the good times, you all are my brothers, and I wouldn't be here without you. See you in California soon.

CONTENTS

LIST OF TABLES

LIST OF FIGURES

INTRODUCTION

Space has long been assumed to be a place of infinite potential. For years, satellite users operated with little concern for adverse externalities over the long term. By the 1980s, groups began to notice that Earth's orbit was becoming cluttered, a problem that continues even today [1]. Fifty years of human presence in space has produced some 30,000 trackable objects in the vicinity of Earth and far more that still cannot be tracked. Of these, NASA claims, only 6% are spacecraft that are currently operational [2]. This minority consists of satellites used for navigation, communications, television, radio, and other missions that positively impact humanity. The functionality is being endangered by the rising threat of damage by debris impact. If not addressed, the threat of debris would likely exponentially propagate to the point of severely crippling the usability of space resources in the near future [3].

One mitigation approach may be to actively attempt to remove current space debris from low-Earth orbit and beyond, such as sending spacecraft to retrieve the debris from orbit. However, active debris removal concepts only address half the problem. Some studies have cited the prohibitive cost requirements of launching specific debris removal hardware, with concepts of tethers or lasers costing in the billions of dollars [3]. A more short-term approach is the effort to prevent the addition of future debris into orbit. One such method, which is still in its infancy, is the application of drag sails to accelerate spacecraft deorbit passively. The concept is applied similarly to a solar sail, but with atmospheric drag considered to be the primary perturbation instead of solar radiation pressure. The intent of the drag sail is to increase the frontal area of a

spacecraft, thus increasing the drag force and allowing it to meet the minimum requirements for reentry time. Practical application of the technology would reduce the time that a spacecraft remains in orbit as debris after their operational lives.

Background

Preserving the space environment for the future requires revisiting the knowledge that has been built up previously. This investigation combines and builds upon three connected but distinct astronautics topics: drag sail design and implementation, space perturbation analysis, and targeted reentry.

Drag Sails

Drag sails have been the subject of increased study in recent years. In the last five years, engineers from both the United Kingdom and Japan have produced test subjects to validate the concept. The Surrey Space Center in the United Kingdom is a leader in drag sail development, having tested DeOrbitSail in 2015 and InflateSail in 2017 to gauge the effectiveness of a drag sail [4][5]. Japan tested its iteration, FREEDOM, in 2016 [6]. Each scenario tested a specifically sized sail with an accompanying CubeSat in low-Earth orbit. The sail size can be small, as Japan's FREEDOM satellite had a sail of only 1 m x 1.5 m on a 1U CubeSat, or much larger, with DeOrbitSail using a 5 m x 5 m sail on a 3U CubeSat, suggesting effectiveness with large variability of test subjects. Figure 1 shows a diagram from the Surrey Space Center of DeOrbitSail configured for various phases of flight. The overall architecture remains similar in all cases, in which a thin polymer sheet is extended into a near-flat surface. These preliminary demonstrations have successfully applied the technology, suggesting that a passive reentry method may be a viable solution for meeting spacecraft deorbiting needs on a larger scale. The

limitation of the current work is that the scenarios proven are fixed to one configuration. To properly apply this technology, a wide array of spacecraft and altitudes must be considered, and this scope of analysis is yet to be fully explored.

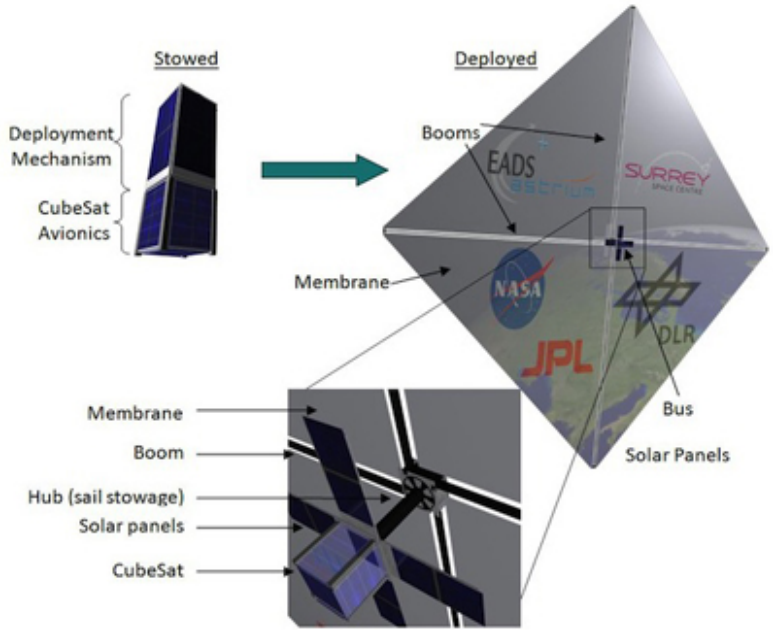

Figure 1. Layout of DeOrbitSail [7]

Perturbation Analysis

High-fidelity analysis of space-based perturbations is a requirement for the application of new drag sail technology. The profile of the high-altitude atmosphere that defines drag weighs heavily on the effectiveness of the drag sails. Since the 1960s, the development of high-altitude atmosphere models has been a significant interest in the space community [8]. Many models have been produced, but no universal consensus has been made for the preferred usage due to the difficulty of the task. Figure 2 shows the historical development of atmosphere models made over the years. A sampling of these, namely the USSA, Jacchia, and DTM models, are considered in subsequent analysis.

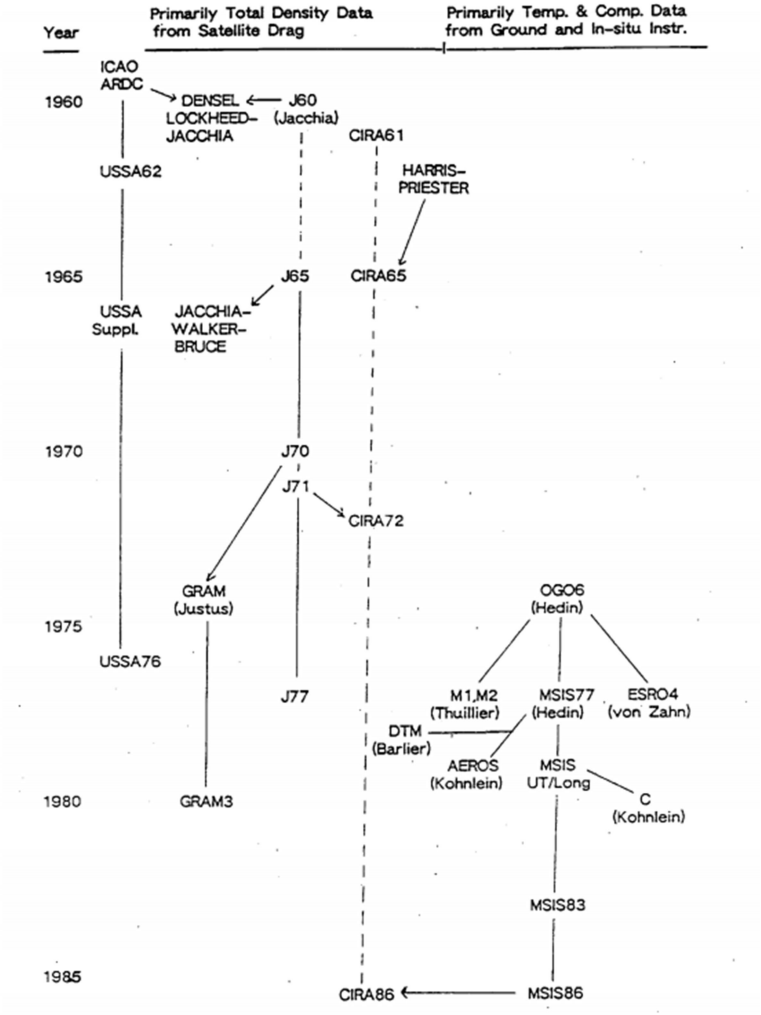

Figure 2. Atmosphere Model Development through the Years [8]

Alternatively, solar radiation pressure is also a well-studied phenomenon that plays a significant role in governing the motion of a spacecraft, in which photons impart a force on the spacecraft that may perturb it along its trajectory. Modern study of solar radiation was performed as early as the late 19th century when the phenomenon was proved to exist theoretically, followed by laboratory tests measuring it in the following years [9]. Spacecraft applications date back to the 1970s when NASA first gained interest in solar sailing [10]. As of 2010, the Japanese-built IKAROS is considered the first complete solar sail-based spacecraft [11]. With the increased

interest in interplanetary travel, solar sailing has surfaced at the forefront of astronautics research and is a major topic of interest for numerous entities worldwide.

While atmospheric drag and solar radiation pressure are at the forefront of perturbation analysis in low-Earth orbit, there is a wide range of other relevant forces that must be considered. Earth's oblateness and third-body effects from other celestial bodies, such as the Sun and Moon, may also result in disturbances that may alter a spacecraft's trajectory. General perturbation analysis for orbits has been a long-studied phenomenon, with solution methods gaining attention throughout the 19th century [12]. High-fidelity perturbation analysis is required to complete propagation for all space-based missions.

Targeted Reentry

For propulsive reentry, targeting a specific location becomes a relatively simple process. With a drag sail, no propulsion is actively being used, thus requiring an in-depth analysis to evaluate and perform targeting. Targeted reentry is vital for a number of mission types, as it is unacceptable to allow a spacecraft to reenter over a heavily populated area, especially if there are components that may not fully break down upon the reentry. Given the novelty of passive reentry, targeted reentry accompanying it is also near infancy.

A few concepts have been evaluated to pursue near-passive targeted reentry. One of the newer ideas uses variable-length booms to attempt reentry targeting from the beginning of the deorbit process, offering more control than an entirely passive scenario. This project, called the Drag Deorbit Device (D3), has suggested that variation of boom lengths on the sail may be used to target reentry; however, the technology is untested and still in its early stages [13]. In 2019, Purdue University researchers presented a system of passive reentry targeting mostly based on

the sail deployment timing to best estimate reentry location [14]. Their claim was that targeted reentry could be fully accomplished by passive means once the spacecraft is within one orbit of reentry using a drag sail. The proposed method leveraged existing technology to induce the reentry.

Requirements

To create a viable application for drag sails on a large scale, specific requirements must be met. NASA and international partners define the maximum amount of time that debris can remain in orbit. Per NASA-STD-8719.14, single non-operational objects in low-Earth orbit must not exceed a 25-year lifetime [15]. This requirement suggests that a satellite has 25 years to be entirely removed from low-Earth orbit from the end of the mission's duration. Additionally, the sum of the lifetimes for all objects for an accompanying mission cannot exceed 100 years. The document also describes the requirements for reentering satellite debris. For controlled reentry, debris of sufficient size must not impact within 50 km of United States soil or permanent ice pack, and 370 km to foreign landmasses. There are also requirements for uncontrolled reentry, stating that the risk of human casualty cannot exceed 1:10,000.

For the scenarios studied, the ideal situation would be an under 25-year deorbit phase that can also meet the distance requirements from land. The risks accompanying uncontrolled deorbit are unclear with the technology used, so targeting a specific region would provide a higher safety level for a specific mission. These two parameters will drive the deorbit analysis for spacecraft presented in this investigation.

METHOD

Effective use of drag sails for passive reentry, while successfully meeting NASA requirements, involves applying a series of relevant engineering principles. The intent of this analysis is to perform a comprehensive study of deorbit methods and lower spacecraft lifetime by leveraging drag sails. The process uses and compares multiple solution methods, different perturbation models, and various initial conditions to ensure the completeness of the analysis. Given the incomplete current state of drag sail technology, CubeSats will be the main focus of the work. CubeSats are a valuable tool for preliminary analysis because of their standardization and ease of use. Preliminary hardware testing would be performed using CubeSats before scaling to larger spacecraft. The behavior of larger operational spacecraft will be taken into consideration. The methods established for lifetime estimation will then be applied to targeted reentry analysis by creating a scenario where a spacecraft's trajectory can be predicted throughout its reentry phase.

Estimation of Spacecraft Lifetime

The initial step to determine orbital lifetime is applying Euler approximation for the integral of time rate of change of the altitude of the orbit. The core process is to solve the orbital period and modify the value based on changes in a time interval to examine how the orbit changes over the long term. The method is ideal for processing large amounts of data quickly. Only drag is considered in the initial analysis due to the relative simplicity of the required equations.

Lifetime Approximation

The initial numerical method for solving orbital lifetime is based on an Euler approximation. The method first requires solving the nominal orbital period, the time it takes for the satellite to complete a single orbit around the Earth. For a given central body, orbital period, P, changes only with the semi-major axis, a, as shown in Equation 1. The gravitational parameter, μ, is defined by the central body and is the ability of the body to exert a gravitational force on other bodies. For Earth, μ is a constant value of 3.986×10^{14} m^3/s^2.

$$P = 2\pi\sqrt{\frac{a^3}{\mu}} \tag{1}$$

Next, the force exerted on the satellite due to drag must be considered. Equation 2 indicates that drag is a function of density for a specific altitude and the dimensions and properties of the spacecraft. The exposed frontal area, A, and drag coefficient, C_d, together define the size and shape of the spacecraft. Atmospheric density, ρ, and velocity, v, are both defined by the altitude. These parameters are then used to evaluate the magnitude of the drag force, D, at a given altitude.

$$D = \frac{1}{2}\rho v^2 A C_d \tag{2}$$

In this analysis, the drag coefficient is fixed at 2.2, which is the most commonly used value for spacecraft [16]. It is assumed that the drag coefficient does not change in the deorbit process, an assumption used for most spacecraft drag analyses. The same consideration is made for the frontal area of the spacecraft. If the spacecraft is tumbling or changing its attitude, the frontal area is continually changing. The effective frontal area is evaluated by finding the

average value of each of the exposed sides. Consider a 3-D rectangular object with side lengths s_1, s_2, and s_3. Equation 3 shows the process for estimating the frontal area of the object.

$$A = \frac{1}{3}(s_1 s_2 + s_1 s_3 + s_2 s_3) \tag{3}$$

The equations for period and drag, along with Newton's second law and the energy of a circular orbit, can be used to derive an expression for the change in period over a time interval. The adjustment factor in Equation 4, *dP/dt*, which is directly used to solve for lifetime, is defined as a function of altitude and spacecraft properties. For a given altitude, spacecraft parameters of size and shape, including mass, *m*, are the primary variables for evaluation. In further analysis, the area-to-mass ratio will be a driving property, given that the drag coefficient is treated as a constant.

$$\frac{dP}{dt} = -3\pi a \rho \left(\frac{AC_d}{m}\right) \tag{4}$$

The final lifetime result is attained by integrating Equation 4, lowering the period for a time step until the spacecraft reaches a pre-established altitude. For the purpose of this investigation, all orbits will be assumed perfectly circular, setting eccentricity equal to zero. This assumption means that the semi-major axis is simply the radius of Earth plus the altitude of the spacecraft.

Many spacecraft in low-Earth orbit do not maintain an eccentric orbit, but in the case of low eccentricities ($e < 0.1$), lifetime can be estimated by applying an effective altitude value into Equations 1-4. Solving for the effective altitude, h_e, requires the use of perigee altitude, h_p, and eccentricity, e, shown in Equation 5 [17].

$$h_e = h_p + 900e^{0.6} \tag{5}$$

The use of an effective altitude assumption is valid for broad estimations more than detailed analysis. Accuracy decreases drastically as the eccentricity increases, especially when the perigee passes close to the Earth, for example, below 200 km. However, given the minimal use of eccentric orbits in the low-Earth orbit region, estimations are sufficient to perform preliminary analysis. The primary focus of the work will be directed towards investigating spacecraft in circular orbits.

Eccentric orbits are a primary limitation of this estimation method using circular orbit calculations for an effective altitude, but the simplicity of the analysis has other drawbacks. First, it is not conducive to the consideration of other perturbations. Drag is considered to be the only force acting on the spacecraft in this initial scenario. The assumption may be acceptable for preliminary analysis but not for specific mission scenarios. Second, Euler approximation does not predict spacecraft location at any given time, making orbit determination impossible without further information. Specifically locating the spacecraft requires numerical integration, which will also be considered.

Atmosphere Estimation

Successfully estimating the lifetime of a spacecraft requires analysis of the space environment. Referring back to Equations 2 and 4, the value for atmospheric density, ρ, is the variable with the highest capacity to change. As such, the most critical factor in determining the reentry time is the atmosphere model used in the calculations. A few atmosphere models exist, referenced in Figure 2; however, the high-altitude atmosphere is not constant over long periods of time due to space environment factors. For the purpose of this study, the models must be simplified and idealized using averages. Note, many atmosphere models are empirical or semi-empirical and may not reflect real changes in the space environment over time.

Software packages such as Systems Tool Kit (STK) have implemented various atmosphere models into their programs, which can then be applied to built-in lifetime calculators [18]. Table 1 compares a few of the more common atmosphere reference models, with lifetime data observed for 24U CubeSats at starting altitudes of 300 and 600 km.

Table 1. Atmosphere Model Comparison using STK Data [18]

	Lifetime	
Atmosphere Model	**300 km**	**600 km**
1976 Standard	63 days	47.9 years
1970 Jacchia	105 days	70.4 years
2012 DTM	116 days	68.0 years

The table reflects the wide variability in total lifetime resulting from different atmosphere models, ranging from 30-40% difference. Nonetheless, each atmosphere model can be used in a meaningful way for a variety of situations. The most common and accessible model used today is the 1976 U.S. Standard Atmosphere.

The 1976 Standard Atmosphere model is typically presented as a table, providing temperature, pressure, viscosity, and air density at specified altitudes [19][20]. This model provides a valid altitude range from sea level up to 1000 km. The model is simple to implement, as density is idealized to singular values with no variability at given altitudes. This simplification has limitations because it does not reflect the changing space environment. Thus, the analysis represents a broad scope but may not be accurate in specific cases. The model reflects the

average state of the space environment over time in order to achieve the most accurate result possible.

Another limitation of the Standard Atmosphere model is that there are no equations for the properties as a function of altitude. Because of the tabular format in which the model is usually presented, numbers are retrieved from a lookup table. Figure 3 shows a typical representation of the Standard Atmosphere model [19]. Observe how at lower altitudes, values are given at 5 km increments. As altitude approaches 1000 km, increments of 100 km or greater may be expected even in the most comprehensive representations [19][20]. Thus, linear interpolation of a table does not provide the necessary data to adequately analyze various scenarios, specifically at higher altitudes. Additional means must be used to further represent the atmosphere model.

Height km	Molec Temp K	Density kg/m³	Density Scale Ht (km)	Pressure N/m²	Pressure Scale Ht(km)	g m/s²
120	380.6	2.440E−08	8.17	2.666E−03	11.58	9.433
125	452.3	1.382E−08	9.51	1.795E−03	13.79	9.418
130	526.9	8.484E−09	11.05	1.283E−03	16.08	9.404
135	600.9	5.563E−09	12.70	9.597E−04	18.37	9.389
140	672.4	3.845E−09	14.44	7.423E−04	20.59	9.375
145	739.8	2774E−09	16.21	5.891E−04	22.69	9.360
150	802.7	2.070E−09	17.98	4.770E−04	24.66	9.346

Figure 3. Sample of 1976 U.S. Standard Atmosphere Data from Literature [19]

The Standard Atmosphere has been extensively studied, and analytical solutions do exist. An example was presented by Brent Lewis from the University of Colorado, Boulder, in 2007 [21]. His solution solves the density of the atmosphere at any given altitude as a function of the atmospheric composition. The program allows for the analysis of the atmosphere at any desired altitude increment, providing sufficient data to consider the full range of altitudes with

acceptable accuracy. The analysis moving forward uses an altitude increment of 1 km in the form of a MATLAB lookup table to create a reasonable balance between the performance of the lifetime calculation codes and accuracy in calculations.

Figure 4 shows the tabular data for the Standard Atmosphere compared to the Lewis solution. A 1% maximum error was cited for the solution [21]. The figure shows that the analytical solution follows the data tables, as apparent from the two curves. The results also highlight that the density decreases exponentially as altitude increases, meaning the orbital lifetime will likely be subject to the same exponential change with altitude, which will be shown in subsequent sections. Note, the density along the x-axis is represented using a logarithmic scale.

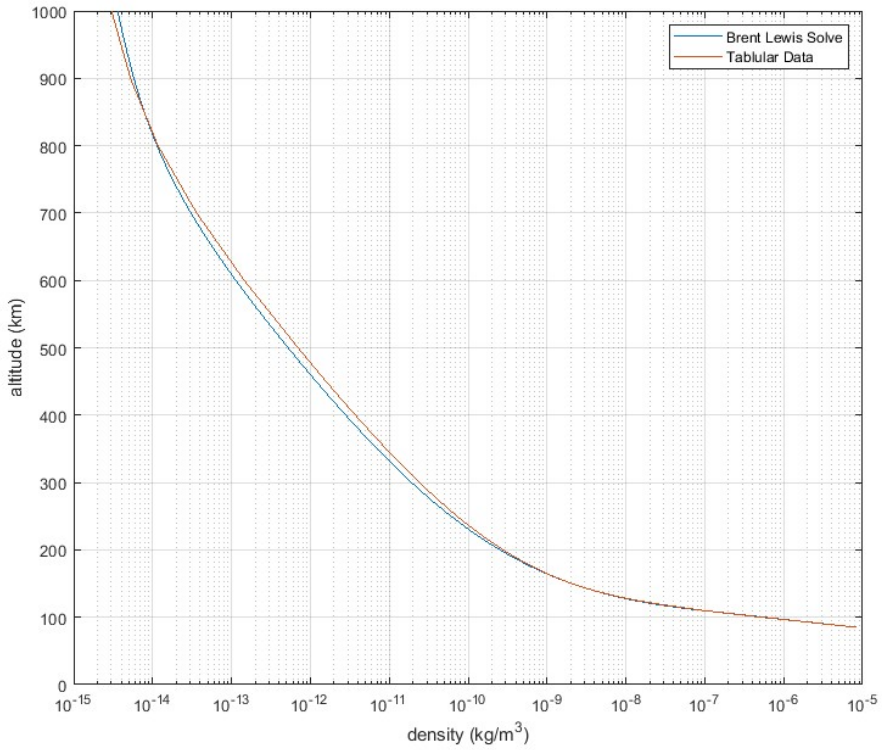

Figure 4. Comparison of 1976 U.S. Standard Atmosphere Data Sets

Other Options for Disposal

To investigate the effectiveness of the drag sail deorbit strategy, the process must be compared to current deorbit methods. Propulsive techniques may be used as an alternative method to deorbit or safely dispose of a spacecraft. There are two ways to properly remove a spacecraft from its orbit using propulsion: targeting a reentry trajectory and allowing it to burn up in the atmosphere or inserting it into a disposal orbit away from operational spacecraft [22].

Both disposal methods can be modeled as impulsive maneuvers, using a single ΔV for reentry or two to enter a disposal orbit. Both methods involve a tangential burn, similar to a Hohmann transfer, although only the first half is performed for a reentry trajectory. The ΔV required is calculated by evaluating the change in velocity at a point in both the initial and final orbits. The process is shown visually in Figure 5. In a circular orbit, the velocity at a given radius, *r*, is shown in Equation 6. This analysis uses a two-body orbit model without additional perturbations. All motion is considered to be in-plane.

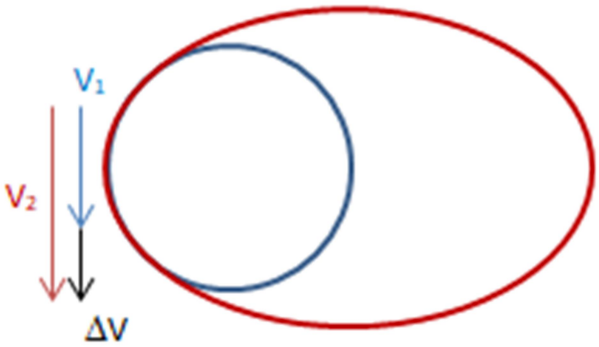

Figure 5. Visual Representation of ΔV Process

$$v_{circ} = \sqrt{\frac{\mu}{r}} \tag{6}$$

The spacecraft performs a maneuver to go from a circular orbit to an elliptical transfer orbit and deliver the spacecraft to its next location. The orbital velocity of an ellipse is governed by Equation 7. It is Equation 6 but with the assumption that radius equals the semi-major axis removed. Equation 7 may be used at any point in the orbit but is calculated primarily at perigee or apogee in the context of a Hohmann transfer. When a reentry trajectory is targeted, the radius is that of the transfer orbit's apogee.

$$v_{ell} = \sqrt{\mu\left(\frac{2}{r} - \frac{1}{a}\right)} \tag{7}$$

Once the initial and desired velocities are found, the total ΔV can be evaluated.

$$\Delta V = v_2 - v_1 \tag{8}$$

Both reentry and disposal orbits are valid options of disposal, and the effectiveness of each depends on the starting altitude. To reenter the atmosphere effectively, the suggested altitude to target is 50 km so that the spacecraft burns up without danger of it skipping off the atmosphere [22]. The disposal orbit, commonly referred to as a graveyard orbit, is an orbit above low-Earth orbit in which the spacecraft will no longer be a threat to operational satellites. Disposal orbits typically begin at 2000 km and can go as high as desired as long as they do not interfere with other commonly used orbits, such as 12-hour medium-Earth orbit or a geosynchronous orbit [22].

Eventually, comparing these methods to a drag sail requires finding the most fuel-efficient current spacecraft disposal method. The two propulsive methods can be directly compared relative to initial spacecraft altitude. Finding the ΔV required to dispose of a spacecraft

is independent of that spacecraft's properties, such as area, mass, and drag coefficient for any Earth orbit. Figure 6 shows the two methods compared based on the starting altitude, ranging from 100 km to 2000 km.

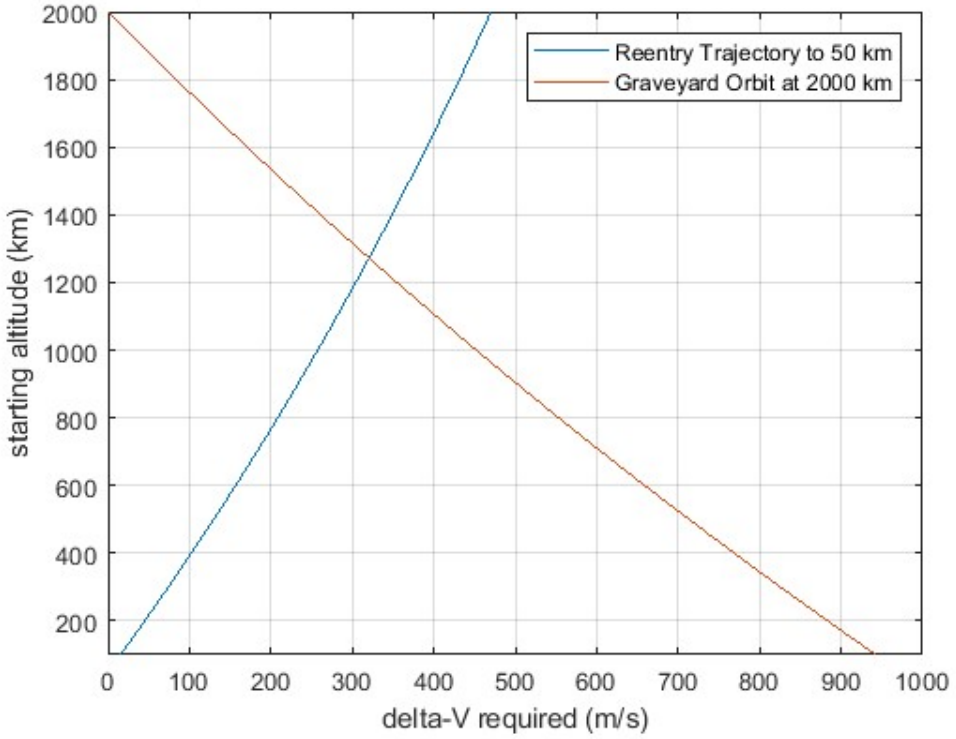

Figure 6. Altitude vs. Required ΔV for Disposal Orbits

Note that until just below 1300 km, atmospheric reentry is the more efficient option, and above that, the disposal orbit is preferable. Given that the Standard Atmosphere model reaches its upper limit at 1000 km, all scenarios considered with a drag sail are compared exclusively to a reentry trajectory. Reentry is more efficient over a broader range of altitudes because it requires only a single impulsive ΔV instead of the two maneuvers required for the disposal orbit.

To analyze this result against the potential performance of a drag sail, an equation is required that relates spacecraft mass to ΔV. The evaluation may be accomplished using the

rocket equation, which is a function of specific impulse, I_{sp}, and acceleration due to gravity, g, shown in Equation 9. Specific impulse is a measure of a rocket engine's efficiency and is primarily dependent on the engine design and propellant used. Chemical rockets may have specific impulses ranging from 250 s to 500 s, and a representative value of 300 s is used in all calculations [23].

$$\Delta V = I_{sp}\, g ln\left(\frac{m}{m_0}\right) \tag{9}$$

The values for m and m_0 refer to the spacecraft's total mass and the empty mass, respectively. To isolate propellant mass, total mass can be separated into components and the equation rearranged, resulting in a ratio of propellant mass to empty mass. This formulation can be used to analyze the propellant required to perform a disposal maneuver for any size spacecraft at a given altitude. Equation 10 is used to find the ratio of propellant mass to the empty mass of a spacecraft. Note that the values of mass are not dependent on spacecraft properties such as area and shape. Figure 7 shows the required propellant mass for the two disposal cases.

$$\frac{m_f}{m_0} = e^{\left(\frac{\Delta V}{I_{sp} g}\right)} - 1 \tag{10}$$

Figure 7, showing relative fuel requirements, reflects the same data trend as Figure 6. Consider the changes to the x-axis data. At the 1300 km threshold, the mass of the propellant exceeds 11% of the spacecraft's empty mass. Considering a satellite's mission fuel usage, this number is a significant measure of effectiveness. Decreasing a mission's life by over 10% may end up saving a significant amount of time and money for replacements or extending the mission. At the USSA's effective threshold at 1000 km, the fuel percentage is about 9%. This

result suggests that if a spacecraft has a mass of 100 kg, it must be holding 9 kg of fuel. This consideration is significant for comparison to drag sail applications.

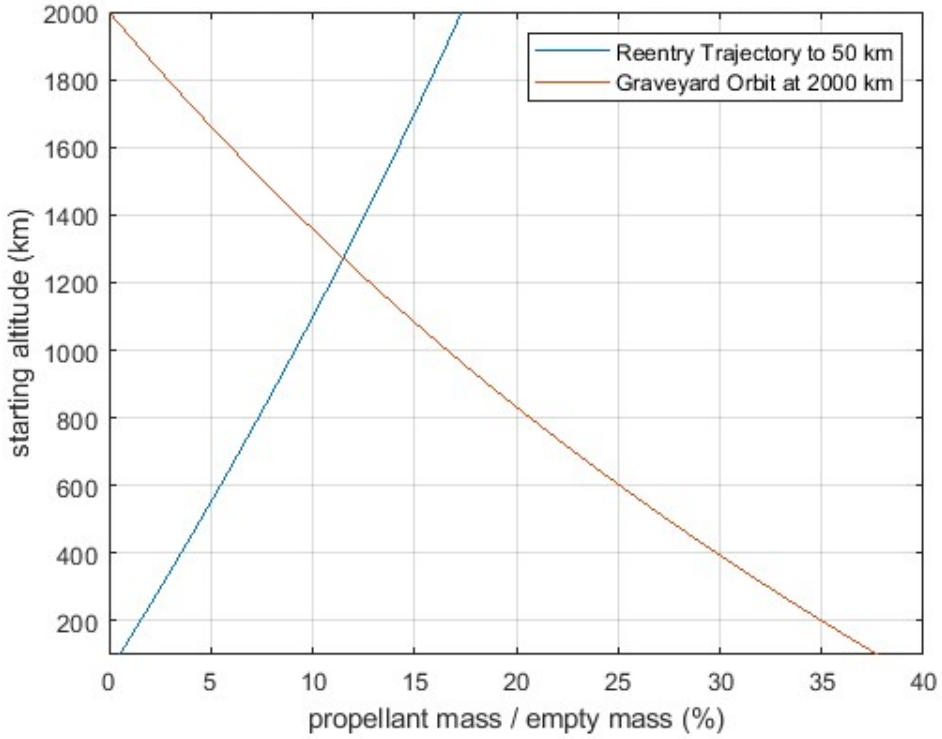

Figure 7. Altitude vs. Propellant-Empty Mass Ratio for Disposal Orbits

Initial Comparison of Drag and SRP

Before a numerically integrated propagator can be implemented, atmospheric drag and solar radiation pressure, commonly referred to as SRP, can be compared for scale. Notably, drag is just one force among a variety of perturbations that affect a spacecraft's orbit over its lifetime. Considering the orders of magnitude of the perturbation accelerations, drag and SRP forces dominate, along with J_2 effects from the Earth's oblateness and third-body effects from the Sun and Moon. Each perturbation provides a different effect on the orbit. Oblateness and third-body effects are largely ineffective on the spacecraft's trajectory given that they contribute only to the

precession of certain orbital elements, such as inclination, right ascension of the ascending node, and argument of perigee. With the changes in the orbital elements, the orbital lifetime should not be affected in a meaningful way. The elements oscillate but will eventually average to the spacecraft's initial state [12].

Solar radiation pressure is more likely to cause a noticeable effect in a spacecraft's lifetime, especially with the significant area increase from drag sails. This is because SRP, along with drag, applies a force that changes the energy of the orbit. R.M. Georgevic, from NASA's Jet Propulsion Laboratory, defined an equation for the force that acts on a satellite from solar radiation pressure in a 1971 report [24]. Equation 11 shows the force exerted on a spacecraft. To compare it to the force of drag, area, A, is moved to the left side of the equation to change the variable to pressure.

$$F_N = \frac{K_{SRP}}{{r_{SP}}^2} A \tag{11}$$

After rearranging the equation to solve for force per unit area, the solution becomes a function of only constants. The radial distance of the Sun to the spacecraft is represented as r_{SP}. Although this value changes as the satellite orbits around the Earth, the change is negligible relative to the distance between the Earth and the Sun and can be ignored in calculations for low-Earth orbit. K_{SRP} is known as the solar radiation constant and is found using Equation 12.

$$K_{SRP} = \frac{(AU)^2 J_0}{c} \tag{12}$$

K_{SRP} is a constant for the Sun, measured in kg*m/s^2. The value is evaluated using a series of additional constants, including the speed of light, c, approximately 3x10^8 m/s, and the astronomical unit, AU, approximately 1.5x10^{11} m, the average distance from the Earth to the

Sun. In addition, the solar constant, J_0, is required. J_0 is equal to 1.353×10^3 W/m^2. Given that K_{SRP} is constant and allowing r_{SP} to be treated as such, the pressure exerted on the spacecraft is constant for a specific orientation. F_N in Equation 11 assumes that the body is normal to the Sun's force, and changing the angle adjusts the force by the cosine of the Sun angle. The orientation of the force is explained in further detail in subsequent sections. Figure 8 compares the pressures from drag and solar radiation.

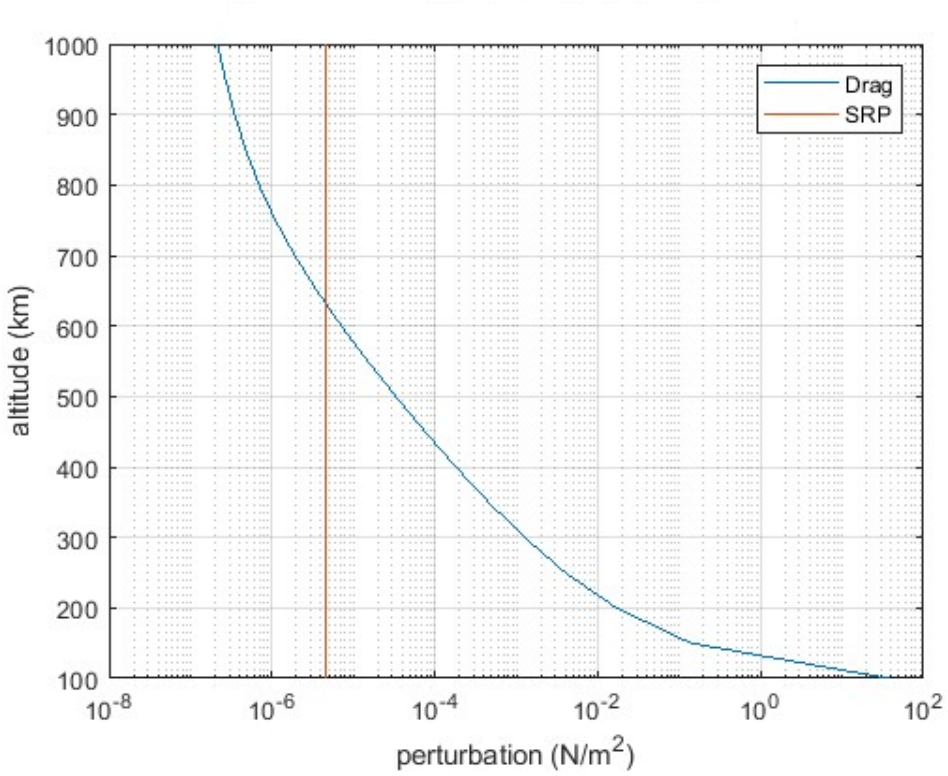

Figure 8. Drag and Solar Radiation Pressure Comparison

Relative to drag, solar radiation becomes the primary perturbing force above 625 km. By 1000 km, SRP exceeds drag by an order of magnitude. For spacecraft in low-Earth orbit with low to moderate inclinations, it must be noted that the spacecraft is in shadow for a significant portion of each orbit when it goes behind Earth relative to the Sun. This, along with the fact that

the spacecraft is not perpendicular to the Sun in all cases, means that the single order of magnitude difference relative to drag at 1000 km does not have the same consistent effect on the spacecraft. SRP only changes the orbital elements periodically and does not significantly change the orbital lifetime for extended propagations [25]. This assumption will continue to be investigated as the problem is further built with numerical integration.

Numerical Integration for Spacecraft Lifetime

The Euler approximation method for evaluating lifetime provides an estimation for large data sets. However, in order to bolster the propagation further, numerical integration must be used. Numerical integration uses differential equations governing the motion of a spacecraft to compute minute changes in the orbital elements from a wider variety of perturbations. For example, the method is more accurate in propagating an eccentric orbit because it reflects real-time changes rather than estimating values like the Euler approximation method. Numerical integration, with greater accuracy in calculation, can be used to validate the initial estimations as well as analyze the changes of specific orbital elements over the lifetime of a spacecraft.

Variation of Parameters

In evaluating a spacecraft's lifetime using numerical integration, the preliminary calculations of perturbation analysis involve applying the Gaussian variation of parameters. The variation of parameters may work with various orbital element sets, but a variation of classical orbital elements is implemented in this analysis. In this case, angular momentum, h, is used in place of the semi-major axis, a, traditionally used in Keplerian mechanics [12]. The remaining elements are eccentricity, e, inclination, i, right ascension of the ascending node, Ω, argument of perigee, ω, and true anomaly, θ. Perturbation, p, is defined relative to the satellite-centric *rsw*

frame, where *r* is the radial vector, *s* is the vector along the direction of motion, and *w* is normal to the orbital plane. The two equations most relevant for this investigation are the Gauss variational equations for angular momentum and eccentricity [12]. Figure 9 shows the orbit with the classical orbital elements and *rsw* frame visually. Equations 13 and 14 show the time derivatives of angular momentum and eccentricity, respectively.

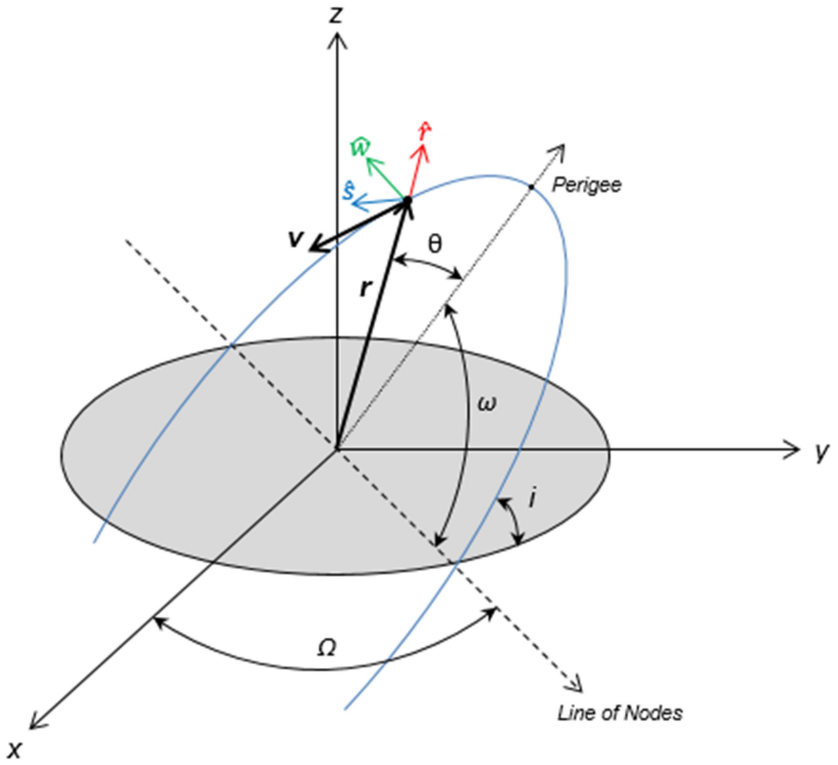

Figure 9. Visualization of Orbit and *rsw* Satellite-Centric Frame

$$\frac{dh}{dt} = rp_s \tag{13}$$

$$\frac{de}{dt} = \frac{h}{\mu} sin\theta p_r + \frac{1}{\mu h}[(h^2 + \mu r)cos\theta + \mu er]p_s \tag{14}$$

Additionally, Equations 15 - 18 show the variational equations for the remaining orbital elements. The variables in Equations 15 - 18 are the angles that define the spacecraft's location,

and additional relevant information about the orbit can be retrieved from them. Refer back to Figure 9 for visualization. Equations 13 - 18 are integrated simultaneously using an ODE calculator, so changes in Equations 15 - 18 directly influence 13 and 14. There is some flexibility as to the specifics of the numerical integration technique. The most significant factor proves to be the tolerances of the solver, given that minute changes in each time step add to significant error over the course of a long propagation.

$$\frac{di}{dt} = \frac{r}{h}\cos(\omega + \theta)\, p_w \tag{15}$$

$$\frac{d\Omega}{dt} = \frac{r}{hsini}\sin(\omega + \theta)\, p_w \tag{16}$$

$$\frac{d\omega}{dt} = -\frac{1}{eh}\left[\frac{h^2}{\mu} cos\theta p_r - \left(r + \frac{h^2}{\mu}\right) sin\theta p_s\right] - \frac{rsin(\omega+\theta)}{htani} p_w \tag{17}$$

$$\frac{d\theta}{dt} = \frac{h}{r^2} + \frac{1}{eh}\left[\frac{h^2}{\mu} cos\theta p_r - \left(r + \frac{h^2}{\mu}\right) sin\theta p_s\right] \tag{18}$$

In the equations, r is the radius of the orbit from the center of the Earth at a given time, and μ is the gravitational parameter of Earth. Additional equations are applied similarly to the remaining orbital elements. The values found in Equations 13 and 14 can then be used to solve for the semi-major axis using Equation 19.

$$a = \frac{h^2}{\mu}\frac{1}{1-e^2} \tag{19}$$

Equations 13 - 18 are integrated to solve for the changes in each element over a specific time interval. Specifically, for the perturbations of drag and solar radiation pressure, the expressions of the scalar value p for all equations must be adjusted with respect to a specific perturbation. First, drag perturbations must be defined to act tangentially to the orbit. The *rsw* frame is adjusted to include only the velocity vector $\boldsymbol{v}$. The perturbation vector $\boldsymbol{p}$ can be

expressed by Equation 20. The magnitude of the perturbation in the velocity vector is shown in Equation 21, where ρ is the atmospheric density, and C_d, A, and m are the drag coefficient, frontal area, and spacecraft mass, respectively. The magnitude of the perturbation force in the direction of the velocity vector is defined as p_v. The perturbation in the direction of velocity shown in Equation 21 is implemented directly into Equation 20 to convert the magnitude into vector form.

$$\mathbf{p} = p_v \frac{\mathbf{v}}{v} \tag{20}$$

$$p_v = -\frac{1}{2}\rho v^2 \left(\frac{C_d A_e}{m}\right) \tag{21}$$

Converting the velocity vector to and from the *rsw* frame requires further evaluation. The velocity vector can be expressed in scalar components of *rsw*, as shown in Equations 22-24. With the components, drag in the direction of velocity can be implemented back into the variational equations.

$$p_r = \frac{\mu}{vh} e p_v sin(\theta) \tag{22}$$

$$p_s = \frac{h}{vr} p_v \tag{23}$$

$$p_w = 0 \tag{24}$$

The drag perturbation can then be solved and combined with the solar radiation pressure perturbation. Concerning solar radiation pressure, the *rsw* coordinate frame is used. The perturbations in each direction, $p_{r,s,w}$, are solved with Equation 25. The values of *SR* in the calculations correspond to the Sun unit vector components in each of the *rsw* coordinate directions, and the magnitude of the perturbing force, p_{SR}, is found with Equation 26. The

perturbing force due to solar radiation is a function of physical spacecraft parameters, with the solar radiation pressure coefficient, C_R, replacing the drag coefficient used in drag perturbation analysis. The solution also requires the speed of light, c, and the solar constant J_0. The shadow function, v, is a binary indicator with the value of one if the spacecraft is in light and zero if it is in eclipse. The value defines whether or not solar radiation is active at a given time along the orbit.

$$p_{r,s,w} = -p_{SR} SR_{r,s,w} \tag{25}$$

$$p_{SR} = v \frac{J_0}{c} \frac{C_R A}{m} \tag{26}$$

Figure 10 shows a simplification of the forces acting on the spacecraft, with drag and SRP highlighted in addition to the sail area. The figure includes a reference to the way the shadow function works with respect to the problem.

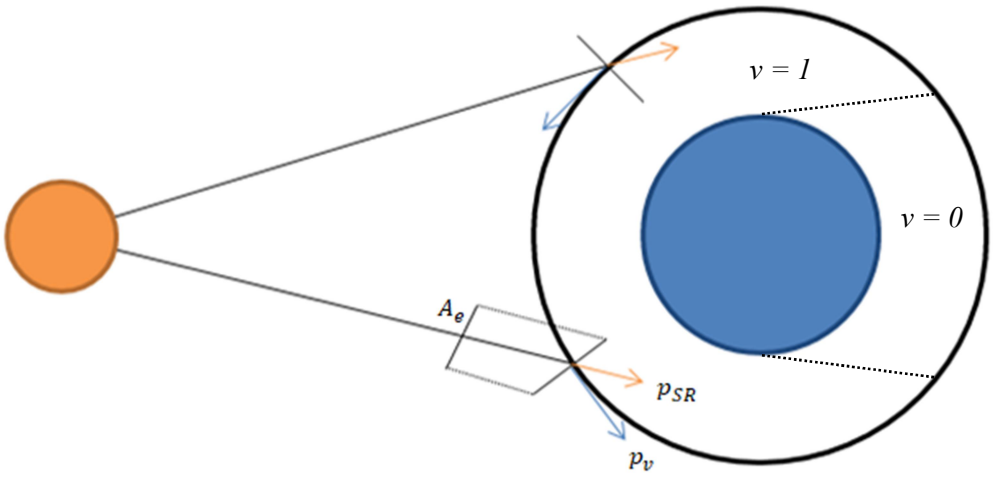

Figure 10. Visualization of Perturbations Acting on the Spacecraft: SRP (p_{SR}) and Drag (p_v)

Solving for the Sun-pointing unit vector from the spacecraft requires applying relevant orbital elements and the parameters defining the location of the Sun. The orbital elements include the right ascension of the ascending node, Ω, and inclination, i, with the solar ecliptic longitude, λ, and obliquity, ε. The argument of latitude is defined as the addition of the argument of perigee and true anomaly and is indicated by u. Each component of the Sun unit vector is a combination of the sines and cosines of these values and can be solved using Equations 27-29.

$$\begin{aligned} SR_r = {} & \sin(\lambda)\cos(\varepsilon)\cos(\Omega)\cos(i)\sin(u) + \sin(\lambda)\cos(\varepsilon)\sin(\Omega)\cos(u) \\ & - \cos(\lambda)\sin(\Omega)\cos(i)\sin(u) + \cos(\lambda)\cos(\Omega)\cos(u) \\ & + \sin(\lambda)\sin(\varepsilon)\sin(i)\sin(u) \end{aligned} \tag{27}$$

$$\begin{aligned} SR_s = {} & \sin(\lambda)\cos(\varepsilon)\cos(\Omega)\cos(i)\cos(u) - \sin(\lambda)\cos(\varepsilon)\sin(\Omega)\sin(u) \\ & - \cos(\lambda)\sin(\Omega)\cos(i)\cos(u) - \cos(\lambda)\cos(\Omega)\sin(u) \\ & + \sin(\lambda)\sin(\varepsilon)\sin(i)\cos(u) \end{aligned} \tag{28}$$

$$SR_w = -\sin(\lambda)\cos(\varepsilon)\cos(\Omega)\sin(i) + \cos(\lambda)\sin(\Omega)\sin(i) + \sin(\lambda)\sin(\varepsilon)\cos(i) \tag{29}$$

Whereas the right ascension of the ascending node, inclination, argument of perigee, and true anomaly are initial conditions for the orbit propagation, solar ecliptic longitude and obliquity must be solved separately. Both of these consider the parameters of the Sun, solar ecliptic longitude and obliquity, to find a solution. First, it is essential to note the time in which the propagation is occurring. Equation 30 quantifies this for use in subsequent equations, using variable n.

$$n = JD - 2451545.0 \tag{30}$$

JD is the Julian date at the start of the propagation, and *n* dictates the number of days since the Julian date at J2000. For the scenarios in this study, the start time is J2000, so *n* in the evaluation is zero.

First, consider the solar ecliptic longitude, which requires using the Sun's mean longitude and mean anomaly, *L* and *M*, respectively. Equation 31 is the solution for λ, and Equations 32 and 33 show the solutions for *L* and *M* as functions of *n*. Each equation can theoretically be above 360° or below 0°; however, they should be bounded within that range.

$$\lambda = L + 1.915° \sin(M) + 0.020° \sin(2M) \tag{31}$$

$$L = 280.459° + 0.98564736° n \tag{32}$$

$$M = 357.529° + 0.98560023° n \tag{33}$$

Obliquity is also only dependent on the time relative to J2000, as seen in Equation 34.

$$\varepsilon = 23.439° - 3.56(10^{-7}) n \tag{34}$$

With the components of SRP solved, Equations 20 and 25 can then be implemented into Equations 13 - 18, filling in the placeholder variables for *p* with the perturbation-specific values to complete the Gauss variational equations with drag and solar radiation pressure. Changes in each orbital element over a long period of time can now be analyzed. In this case, changes over the entire orbital lifetime of the spacecraft are the point of interest.

The numerical integration method could then be expanded upon for all required perturbations for a given scenario. The numerical integration method is powerful because it is an overarching solution for perturbation analysis and orbit propagation. As such, a more in-depth analysis could incorporate J_2 and third-body effects, which will be discussed later.

Drag Sail Attitude

When analyzing perturbations, the orientation of the spacecraft in orbit is an important parameter to consider. From Equations 21 and 26, it is apparent that the exposed frontal area is a relevant variable when performing the calculations. For a CubeSat with a constant area assumption, the value for the frontal area used in both drag and SRP calculations are the same. However, this assumption is invalidated when drag sail models are implemented into the dynamical framework. Given a large, nearly flat surface like a drag sail, the effective frontal area, specifically relative to solar radiation pressure, can change drastically as the spacecraft moves around the Earth.

First, consider Equation 21, which uses the effective frontal area, A, to calculate the ballistic coefficient of the spacecraft, the term in the parenthesis. In the case of drag, the frontal area is the area of the sail normal to the velocity vector, which is the entire area of the sail if the attitude of the sail is not changed. This assumption is not the case for solar radiation pressure, however. The sail does not have a consistent orientation relative to the SRP perturbation vector. Instead, the effect of SRP is continuously changing due to the change of the Sun vector relative to the spacecraft's orientation along its trajectory.

Having already calculated the Sun vector using Equation 25, a vector for velocity must be found. Previously, velocity had been shown as vector $\boldsymbol{v}$; however, it must be converted to the *rsw* frame to relate it to the Sun vector. This process begins by solving for the flight path angle, φ, at any given point of the orbit as a function of eccentricity and true anomaly, shown in Equation 35.

$$\varphi = tan^{-1}\left(\frac{esin\theta}{1+eco}\right) \tag{35}$$

Eccentricity and true anomaly can be defined at any point by modifying the initial conditions from the results of Equations 14 and 18, respectively. The flight path angle can then be used to convert the known magnitude of velocity into components of *r* and *s*. The normal component, *w*, is not represented due to the in-plane motion. For further calculations, velocity must be a unit vector to ensure that dimensional units cancel each other. In the case of the unit vectors for drag and SRP, the angle between them is referred to as the angle of attack, α. This angle can be solved by manipulating the dot product formula, shown in Equation 36.

$$\alpha = cos^{-1} \frac{\boldsymbol{v_u} \cdot \boldsymbol{SR}}{|\boldsymbol{v_u}||\boldsymbol{SR}|} \tag{36}$$

With the angle of attack, α, the effective sail area can be evaluated relative to the Sun. Thus, solar radiation pressure acting on the spacecraft can be represented more realistically rather than merely using the full area of the sail as area value, *A*, in Equation 26. As the spacecraft moves along its trajectory, the exposed frontal area is the sail's total area multiplied by the cosine of the angle of attack. Figure 10 shows the way the exposed frontal area, A_e, appears with respect to the orbit. The effective area is the only variable that changes as the spacecraft attitude changes. Other variables in Equation 26, including the physical constants of the Earth and Sun and spacecraft specifications, such as solar radiation pressure coefficient and mass, are considered to be constant throughout the spacecraft's lifetime. Figure 11 shows a visualization of the attitude of a spacecraft in orbit.

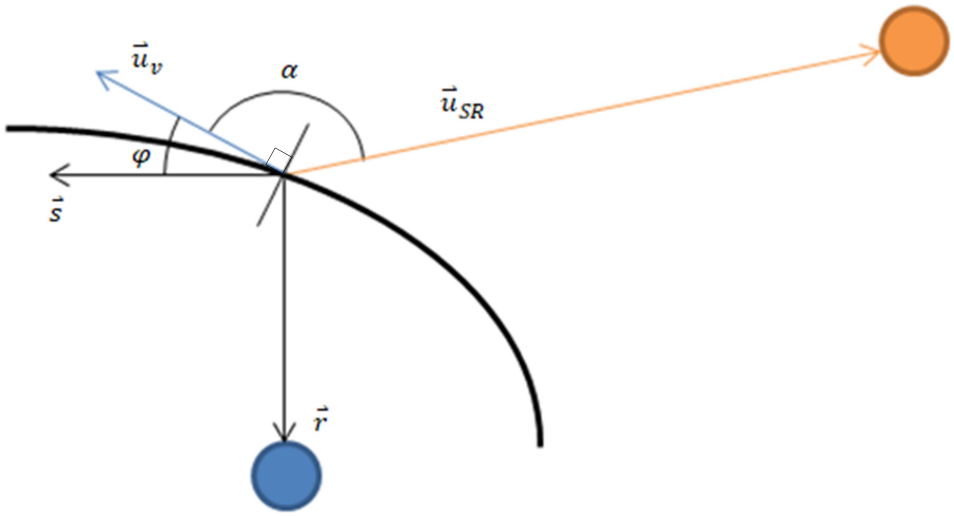

Figure 11. Visualization of Attitude of a Spacecraft in Orbit

When planning for the attitude control of a passive spacecraft, stability becomes a concern. Studies have shown that spacecraft with drag sails are inherently unstable [26]. Therefore, it is not acceptable to simply deploy the sail and commence deorbit without additional consideration, given the fact that the spacecraft may significantly tumble throughout its reentry, rendering the analysis invalid. Although stability will not be a topic discussed, research has shown that stability of a spacecraft operating passively with a drag sail can be attained under the right circumstances and construction [26].

Eclipse Ramifications

As a spacecraft moves around the Earth, there are times that the spacecraft is eclipsed from the Sun by the Earth. As a result, solar radiation pressure does not constantly act on the spacecraft. In Equation 26, the eclipse time is dictated by only one variable, shadow function *v*,

which dictates whether the spacecraft is subjected to SRP forces. For initial analysis, v is fixed at 1, which means that the spacecraft is always in sunlight. Although this does not necessarily represent realistic scenarios, it is essential to view the maximum potential effect of the Sun on the spacecraft. Additionally, this assumption minimizes the impact on changes to initial orbital elements, given that spacecraft position, starting time, and location are not relevant factors in the analysis of eclipses. Some analysis on eclipse will be made; however, the assumption is of constant solar radiation pressure acting on the spacecraft when initially considering solar radiation pressure effects and their magnitude relative to drag.

J_2 Perturbation Effects

One additional perturbation considered that has the potential to significantly change an orbit near Earth are J_2 oblateness effects. This perturbation stems from the fact that the Earth is not a perfect sphere. Instead, it could be referred to as an oblate spheroid, given that the radius is smaller at the poles than at the equator by approximately 21 km. The discrepancy means that the gravity field is not consistent throughout the orbit and leads to a drift in the orbital elements [12]. The right ascension of the ascending node, Ω, and argument of perigee, ω, are the two elements that undergo an immediate change, with average rates being shown in Equations 37 and 38.

$$\frac{d\Omega}{dt} = -\left[\frac{3}{2}\frac{\sqrt{\mu}J_2{R_E}^2}{(1-e^2)^2\bar{a^7}}\right]cosi \tag{37}$$

$$\frac{d\omega}{dt} = -\left[\frac{3}{2}\frac{\sqrt{\mu}J_2{R_E}^2}{(1-e^2)^2\bar{a^7}}\right]\left(\frac{5}{2}sin^2i - 2\right) \tag{38}$$

The value of J_2 is a dimensionless constant dependent on the relevant central body. Note that these rates refer to the average changes over time. The equations rely on the other orbital elements, namely the semi-major axis, a, eccentricity, e, and inclination, i, despite these elements

not undergoing any significant changes themselves throughout the orbit. Energy in the orbit, which can be considered with the semi-major axis or angular momentum, is not affected by the J_2 equations. As such, J_2 should not cause any changes to the overall lifetime of the spacecraft on its own. From a lifetime standpoint, the effects of oblateness are relevant because it would begin to change these orbital elements, which would then have the potential to drive changes in the other orbital elements when integrating Equations 13-18. Moving forward, the expectation is that J_2 affects the orbit positioning but not the lifetime due to failing to increase or decrease the orbit's energy.

Targeted Reentry

To complete the analysis on passive drag sails, the process of specific reentry targeting is of vital importance. As stated earlier, targeted reentry must meet minimum distance requirements relative to areas of land. Thus, the spacecraft must be able to reenter in a way that meets the criteria while still maintaining the passive nature of the deorbit process. If sufficient propulsion is used to subsidize the targeting limitations of a drag sail, the additional fuel usage defeats the purpose of the passive process.

Two considerations are made to target the reentry of a spacecraft. First, the altitude from which targeting can be achieved must be found; then, the specific location of reentry must be considered. Together, these elements cover the error that may be expected of a spacecraft and specific locational concerns, meeting all criteria from a safety standpoint.

Maximum Targeting Altitude

The main focus of the process of passive targeting is determining the maximum altitude from which the drag sail can be deployed to reenter within the target range. The starting point for this solution is the intended final state of the orbit, and the initial orbit parameters are solved through backtracking. In this case, the longitude range within which deorbit is acceptable for the intended scenario is the starting point for the solution. The targeting longitude is mission-dependent and varies based on the location of the intended reentry, with any range valid up to about 90°, which is generally the full usable span of the Pacific Ocean. A specific target for reentry is selected, a center point of the intended range, and then the total range is predicted based on the assumption that all orbits are subject to a 10% random error in predictions [17]. The 10% error pertains to the satellite's total lifetime, which can be evaluated knowing the initial altitude and spacecraft parameters. First, the spacecraft state must be considered immediately before reentry. The assumption is that the spacecraft is considered deorbited when the altitude reaches 86 km, representing the shift from a low-altitude to a high-altitude atmosphere in the 1976 Standard Atmosphere model. That is, minimum additional longitudinal progression is observed when the satellite reaches the 86 km altitude threshold [19]. At an altitude of 86 km, it is essential to know the period of the orbit, which can be solved by referring back to Equation 1.

At an altitude of 86 km, the orbital period is about 86 minutes, assuming a circular orbit. Knowing this information, the distance the spacecraft drifts away from the target center-point can be found. For example, if the satellite is allowed a 30° reentry corridor, it will take a twelfth of the orbital period to cross from one end of the corridor to the other. This value results in a time of 7 minutes, 10 seconds. Measured from the expected center point, this means the ends of the range are 3 minutes, 35 seconds in each direction from the center point. The time can be

considered synonymous with the 10% expected error for all deorbiting spacecraft. Given this assumption, the scenario yields a maximum deorbit time of about 36 minutes to safely expect the debris to reenter within the corridor from any relevant initial altitude. The acceptable time changes exclusively with the intended reentry corridor and defines the maximum time that any satellite can spend in orbit to meet the requirements. The appearance of the reentry corridors on an Earth ground track is shown in Figure 12.

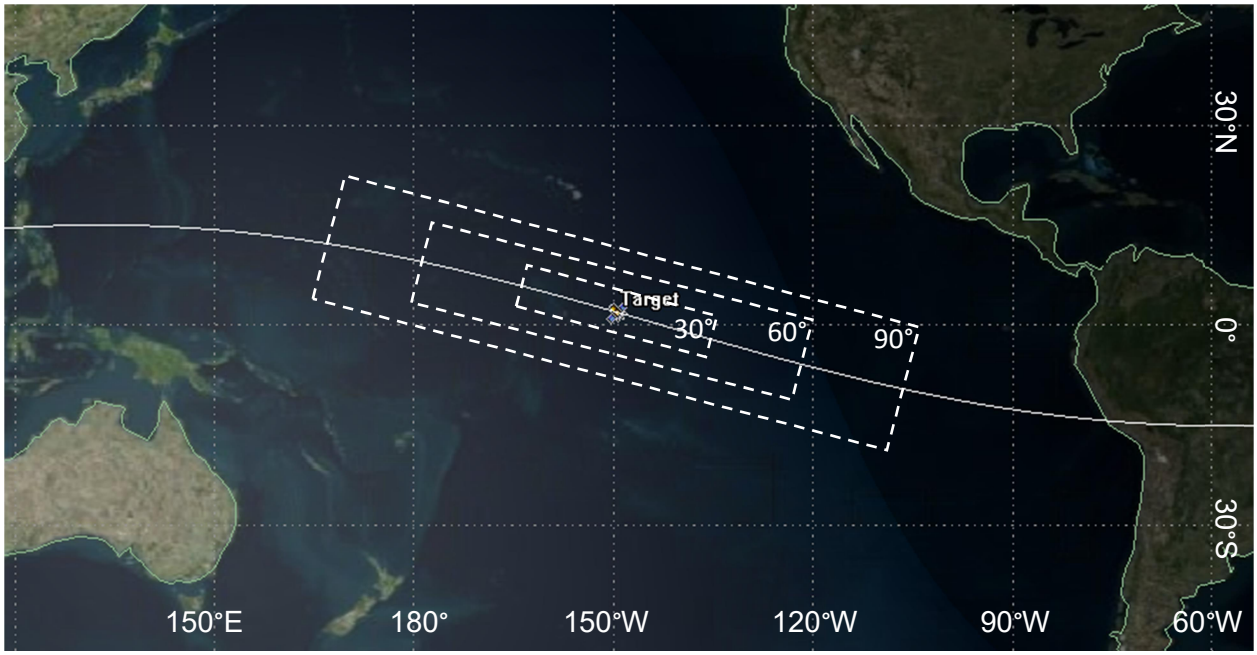

Figure 12. Example Reentry Corridors [18]

Equation 4 is again used to find the spacecraft lifetime. Knowing the maximum allowable deorbit time and the method for finding individual scenario deorbit times, maximum altitude for all cases can be found. Equation 4 cannot be applied in reverse to find the starting altitude, and the process for finding altitudes should instead start with a best estimate based on the initial conditions. It is then integrated until the deorbit time matches the maximum allowable. CubeSats are the primary focus in this investigation, with some consideration for larger, operational

spacecraft. The method based on the longitude range differs from the maximum targeting altitude study as the conditions for reentering are not fixed [14]. The mission requirements and potential recovery of the spacecraft components pose as the governing factors for deorbit starting parameters.

Latitude/Longitude Targeting

Finding the altitudes necessary for a targeted reentry along a corridor is an essential first step in solving the passive reentry problem, but it is arbitrary unless the specific locations on the Earth to target are known. The critical values to consider are the latitude and longitude of the projected impact point, which can be used to safely consider the ramifications of spacecraft components hitting the ground and to meet the 50-370 km minimum distance dictated by NASA. The parameters for the initial conditions are calculated in the Cartesian ECI coordinate frame, which is one of the standard orbital element sets when the orbit is propagated with numerical integration. Although these calculations use Cartesian ECI, simple conversions are available from the Keplerian elements primarily used in this investigation. NASA has documented the method for converting the spacecraft location, referred to as sub-satellite points, from the orbital elements [27].

Latitude is the first sub-satellite point to consider. Latitude is independent of the Earth's rotation and bounded by the satellite orbit's inclination, i. This rule means that if a spacecraft is orbiting with an inclination of 30°, latitude, Φ, is always approximately $-30° \leq \Phi \leq 30°$. An important distinction, however, is that the latitude can be considered in two different ways. The first and most straightforward way is to treat the Earth as a perfect sphere. This measurement is called the geocentric latitude and is measured as the angle from the equatorial plane to the spacecraft's radius vector. However, most modern cartography systems account for the Earth's

oblateness and instead adjust the latitude to reflect the variation [28]. The modified value is called the geodetic latitude, and the distinction is shown in Figure 13. The Earth, represented in blue, is exaggerated for clarity relative to the circle in red.

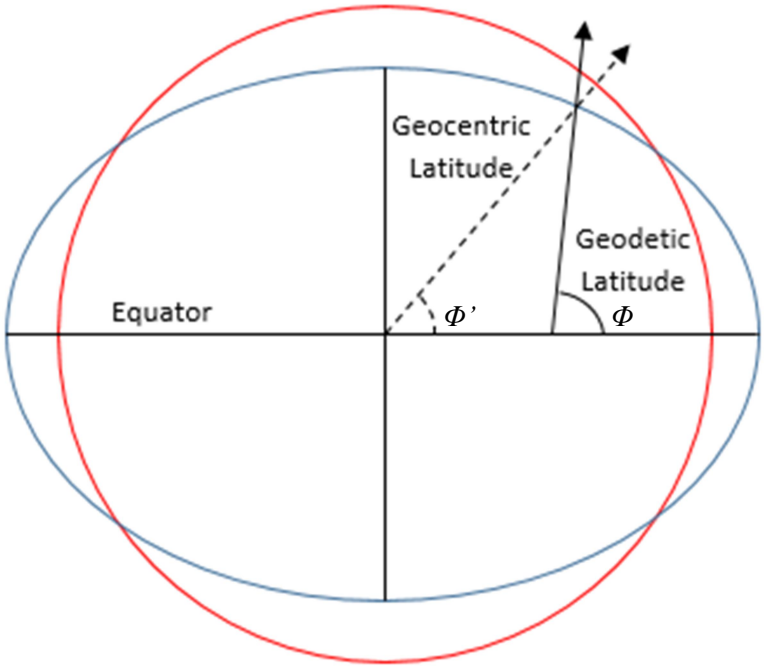

Figure 13. Geocentric vs. Geodetic Latitude

The value of the geodetic longitude can be evaluated from the orbital elements, starting with the geocentric latitude. The geocentric latitude, Φ', is found calculated with the radial components, x, y, and z, of the Cartesian orbital elements and can be found using Equation 39.

$$\Phi' = tan^{-1}\left(\frac{z}{\sqrt{x^2+y^2}}\right) \tag{39}$$

Knowing the geocentric latitude, the conversion can be made to find the geodetic latitude. Per NASA documentation, the conversion involves taking the geocentric latitude and adding the first two terms of a series expansion to best represent the changes for Earth's oblateness. The

difference is small but crucial in accurately representing the locations of objects on the Earth's surface. Equation 40 shows the process of converting geocentric to geodetic latitude, Φ.

$$\Phi = \Phi' + a_2 \sin(2\Phi') + a_4 \sin(4\Phi') \quad (40)$$

In the equation, a_2 and a_4 are the first two terms in the expansion required for the conversion. Equations 41 and 42 show how to solve for a_2 and a_4, respectively.

$$a_2 = \frac{1}{1024r}(512\hat{e}^2 + 128\hat{e}^4 + 60\hat{e}^6 + 35\hat{e}^8) + \frac{1}{32r^2}(\hat{e}^6 + \hat{e}^8) - \frac{3}{256r^3}(4\hat{e}^6 + 3\hat{e}^8) \quad (41)$$

$$a_4 = -\frac{1}{1024r}(64\hat{e}^4 + 48\hat{e}^6 + 35\hat{e}^8) + \frac{1}{16r^2}(4\hat{e}^4 + 2\hat{e}^6 + \hat{e}^8) + \frac{15\hat{e}^8}{256r^3} - \frac{\hat{e}^8}{16r^4} \quad (42)$$

These solutions rely on the magnitude of the radius, r, and the eccentricity of the Earth spheroid, $\hat{e}$. The eccentricity, per World Geodetic System (WGS) 84, is approximately 8.1819×10^{-2} [28].

The other sub-satellite point is the longitude. Longitude, measured around the equator, is vital because it is the main factor in targeting large, safe areas such as oceans. Additionally, longitude is not subject to the same conversion ramifications as latitude. Like latitude, the solution begins with finding relevant parameters from the Cartesian orbital elements. The first such parameter is the right ascension, RA, which can be found using Equation 43.

$$RA = tan^{-1}\left(\frac{y}{x}\right) \quad (43)$$

Unlike latitude, the right ascension does not rely on the z component of the radius. Longitude can be considered exclusively in the equatorial plane.

Right ascension is the only value that must explicitly be found when solving for the longitude. Equation 44 shows the solution for longitude, λ.

$$\lambda = RA - \lambda_0 - \widehat{\omega}\Delta t \quad (44)$$

The other variables are a combination of constants and values that are case-dependent. The rotation rate of the Earth, $\hat{\omega}$, is treated as a constant, at about 7.3×10^{-5} rad/s. The time value, *t*, can be found from the length of the propagation. However, the equation assumes that the starting value of longitude is known. In most cases, this is a mission-dependent decision and can be adjusted to meet the needs of the scenario.

The sub-satellite points, latitude and longitude, are used to find the spacecraft's location above the Earth at any given time. In most cases, the starting and final positions are the states that are most important for analysis. The final state is used to find the reentry target, determining whether the deorbit requirements are met. This knowledge can be used to retroactively determine the initial state from which the deorbit sequence would be initiated. The initial and final states, in conjunction with the determination of maximum altitude from the intended reentry corridor, are sufficient to analyze reentry needs for most spacecraft in low-Earth orbit.

RESULTS

Having discussed the method of analysis for the implementation of drag sails in orbit, this section will focus on the data resulting from the application of the process. CubeSats will serve as the initial platform for analysis, with various other spacecraft representing examples of missions that may benefit from the drag sail study. In addition to analyzing the usability of drag sails, some analysis of the system's monetary cost will be performed to verify if the method is relatively cost-effective. The results are split into three sections: consideration of large amounts of data using the Euler approximation lifetime solution, verifying the effects of other perturbations in the system, and targeting reentry locations on Earth. The data will be presented with a few initial responses and discussion.

Orbital Lifetime

For the first phase, the resulting lifetimes from the Euler approximation method are to be considered. The method allows for quickly processing a large number of variables, including altitude and spacecraft size. Tolerances for the numerical method are scaled based on the initial altitude, ranging from 10^{-3} to 10^{-6}. The resulting data dictates the formation of initial conclusions about drag sail reentry. Several comparisons will be made initially to reenter the atmosphere based on the spacecraft's default configuration. Additional comparisons to the previously discussed propulsive disposal methods, with mass and cost considerations, are to be presented. Alternatively, the discussion will address how much a sail would need to be scaled to meet the minimum requirements for deorbit in the 25-year limit.

CubeSats

The analysis was initially performed on five CubeSats of different sizes: 1U, 3U, 6U, 12U, and 24U [29]. The frontal area and mass vary between each configuration. A few assumptions were made in this preliminary investigation phase. First, all orbits are assumed to be circular. Spacecraft were assumed to deorbit when the altitude decreased below 86 km. Additionally, drag is the only perturbation acting on the satellites, with no solar radiation pressure or other space environment effects. A drag sail is assumed to be perfectly perpendicular to the direction of the velocity vector at all times. Constant mass and area assumptions are also made. When considering the cases with drag sails, the dimensions are assumed to be 5 m x 5 m, resulting in an effective area of 25 m^2. Figure 14 shows a simplified version of what a 24U CubeSat may look like, with each cube in the figure having 10 cm sides.

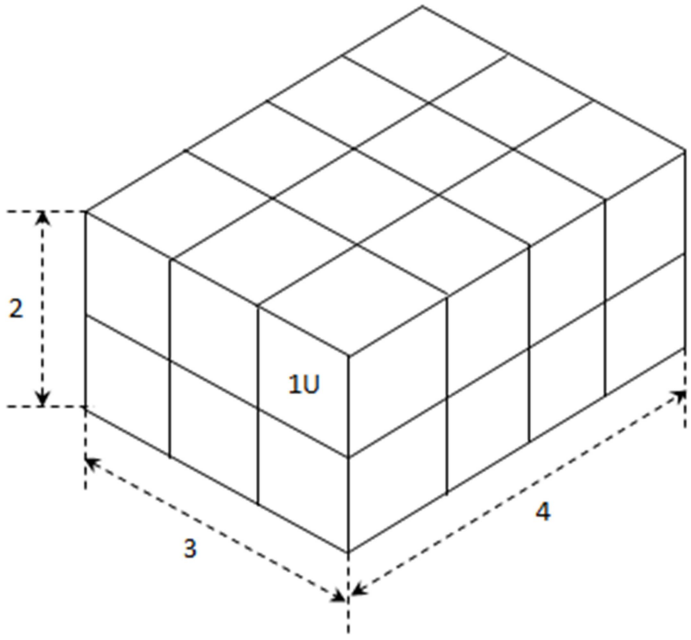

Figure 14. Simplified 24U CubeSat Representation

The number before the U in each CubeSat configuration refers to how many of the 1U building blocks are built into the final size [29]. A 6U, for example, may consist of dimensions of 1x2x3. Theoretically, any combination of these components could be feasible; however, some standardization is apparent. The 5 CubeSats represented in this study are commonly used configurations. The interest in CubeSats is that they are cheap, modular, and easy to operate. Instead of investing millions of dollars on a full-sized test platform for new technologies, CubeSats can be used to complete test missions with significantly lower risk. Not only do CubeSats drive the cost down in spacecraft construction, but one can be easily stowed away as a secondary payload on a larger mission.

The first case considered involves each CubeSat's default configuration, with no additional drag surfaces. The five CubeSat configurations were analyzed at a 100 km to 1000 km altitude range in 50 km increments. In Figure 15, the solid lines show the resulting times of the analysis, found using Equation 4. Because of the significant discrepancy in times for the upper and lower limits of the range, over 4000 years at 1000 km and mere hours at 100 km, a logarithmic scale is used for all lifetime plots. Values were verified using preexisting documented work, including the STK software package's lifetime tool.

Note that the times to deorbit generally surpass the 25-year maximum, primarily above 500 km. The larger CubeSats deorbit noticeably later than smaller sizes. A 1U CubeSat is the low-end of the technological limitations, tested with Japan's FREEDOM satellite [6]. DeOrbitSail serves more as the benchmark for this work with a 25 m^2 sail on a 3U CubeSat [4]. At higher altitudes, above about 800 km, the CubeSats orbit for longer than 1000 years. Many near-Earth satellites orbit in the 700 to 800 km range, validating the need to accelerate the deorbit strategy.

Next, a drag sail is included in the analysis. The drag sail is presented in a simplified manner, using constant area and attitude assumptions. The assumptions may conflict with the substantial amounts of solar radiation effects; however, they simplify the preliminary work. Note that the sail size is constant for all cases, while each CubeSat's mass varies based on its respective size. Smaller CubeSats undergo a greater relative change in area-to-mass ratio than the larger CubeSats. Even the 24U CubeSat only has an area of 0.086667 m^2, so the 25 m^2 sail is a massive increase regardless. The dashed lines in Figure 15 shows the deorbit times for each CubeSat using a drag sail.

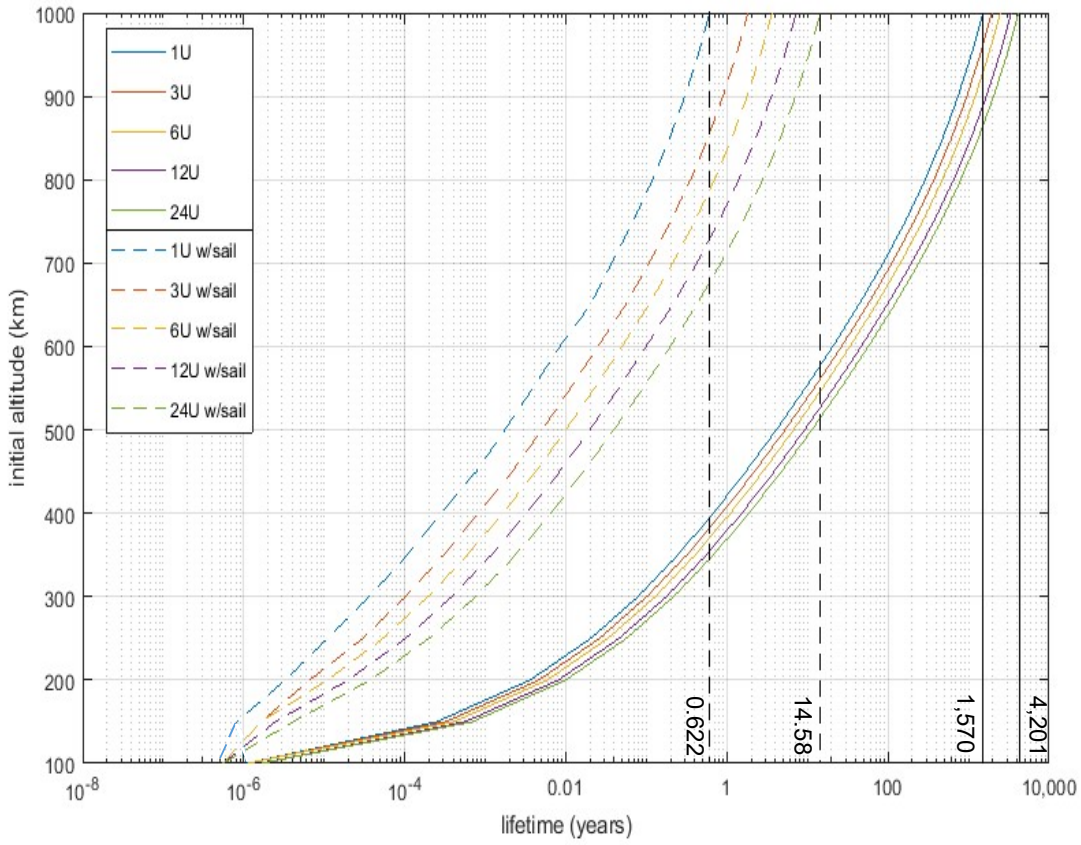

Figure 15. Orbital Lifetime Data for Circular Orbits, with and without Drag Sails

The most apparent result of comparing the two cases is the drastic decrease in the total time spent in orbit for all situations. In all the drag sail example cases, the lifetime is below the 25-year mark, with the longest time being about 15 years. This result displays promising results for using the drag sail concept in deorbiting CubeSats and potentially larger spacecraft. The drastic decrease in lifetime is due to the significant increase in the effective frontal area that leverages the increased force of atmospheric drag to accelerate deorbit. A standard 1U CubeSat has dimensions of 10 cm x 10 cm. Applying a 25 m^2 drag sail increases the effective area by a factor of 2500. For a 24U CubeSat, the relative change in area is much smaller but nonetheless substantial, nearly reaching 300 times the size. For a low-mass spacecraft, the results indicate a drastic decrease in deorbit time. Further analysis is warranted, as the drag sail concept appears to be an effective method of decreasing a satellite's deorbit time.

The eccentricity of the orbit is another relevant factor when calculating the orbital lifetime. Differences in orbital lifetime for eccentric orbits require using the effective altitude while performing the calculations consistent with a circular orbit. The effective altitude represents an average value of the altitude based on its shape and is valid at low eccentricities [17]. The eccentricity values studied in this investigation range from 0.02 to 0.08. Figure 16 represents the lifetimes of a 24U CubeSat without and with a sail for various eccentricities. The zero eccentricity case is shown for reference. The 24U CubeSat is used because it has the longest deorbit times, shown in Figure 14, and therefore the least likely to be immediately affected by error. The altitude on the y-axis is an average altitude, found by subtracting the Earth's radius from the semi-major axis. This calculation presents a direct comparison to the circular orbit case.

First, note that the lifetimes for spacecraft in high eccentricity orbits are not feasible down to 100 km altitude. The reason is that, at higher eccentricities, the spacecraft's perigee is

very close to Earth and reenters in less than one orbit due to the large drag force. An inverse relationship is evident from Figures 16, conveying that lifetime decreases as eccentricity increases. This behavior is apparent because, as eccentricity increases, the spacecraft spends a greater duration of its orbit in low altitude, subject to higher drag. The increased forces at low altitudes have a more significant effect on the orbital lifetime than the additional time spent at a higher altitude due to the exponential nature of the atmosphere model.

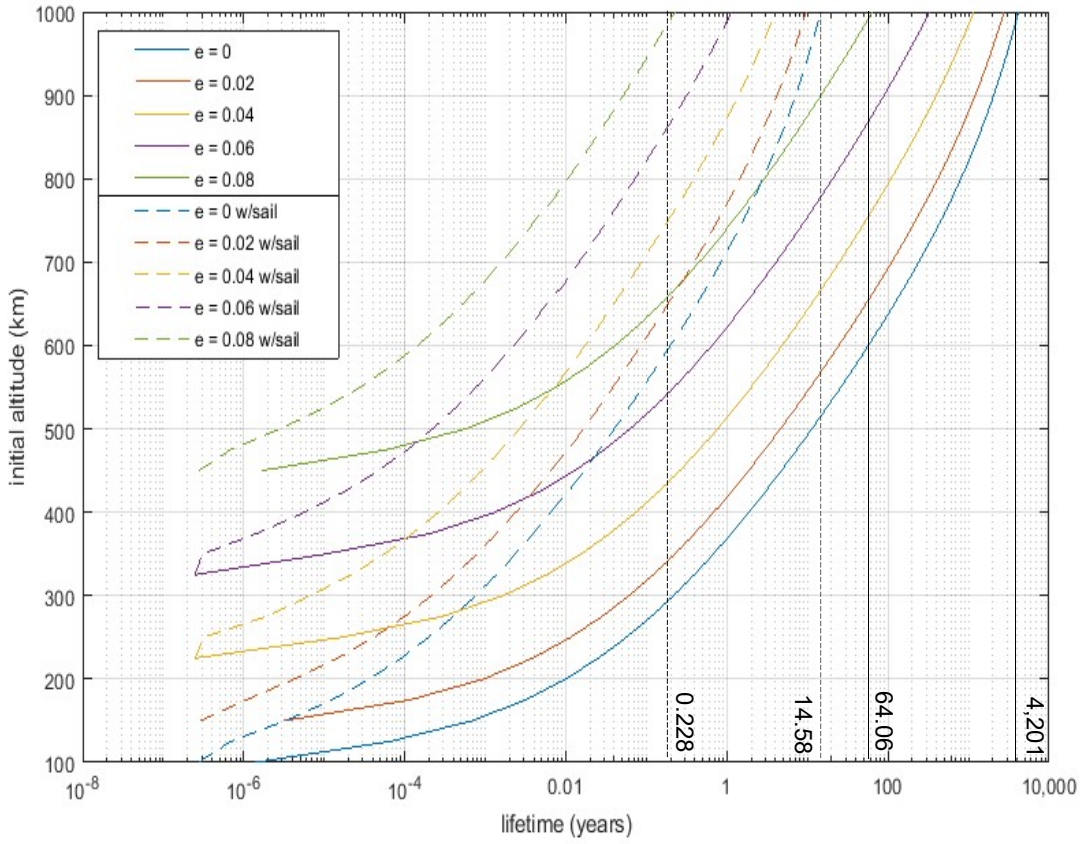

Figure 16. Orbital Lifetime Data by Eccentricity, 24U CubeSat

Adding a drag sail to a spacecraft in an eccentric orbit results in the same effect shown in circular orbits. Despite the decrease in orbital lifetime shown by greater eccentricity, the higher eccentricity values still result in lifetimes barely below 100 years. However, a drag sail can

exaggerate the effect, and as a result, the orbital lifetime falls below one year with eccentricities above 0.05, even from 1000 km altitude. The decrease in lifetime by increasing the eccentricity is a meaningful result. In addition, the circular orbits have longer deorbit times. The difference suggests that some perturbations to the eccentricity do not invalidate the circular orbit investigation results. Note that there are few situations in which it is important to maintain high eccentricity in a low-Earth orbit, but all satellites are subject to perturbing forces that prevent a spacecraft from maintaining a perfectly circular orbit. For significantly higher eccentricities, such as those used in many polar observation satellites, numerical integration may be required to represent the orbit accurately.

Sail Scaling to 25-year Lifetimes

With the data suggesting that CubeSats deorbit in significantly less than 25 years with a 25 m^2 sail, the drag sails can be scaled to target a deorbit in precisely 25 years. Targeting a 25-year reentry would decrease the sail size and save mass and, therefore, increase cost-effectiveness when planning end-of-life operations for a spacecraft without failing to meet the deorbit requirements. Calculations are simplified by the fact that the lifetime is directly proportional to the frontal area. For example, doubling the sail's size would cut the lifetime in half, apparent from Equation 4. This knowledge can be leveraged to scale a drag sail if the initial area is known, and the lifetime is solved using the updated area. The sail is scaled as a percentage of the observed lifetime over the intended lifetime. The intended lifetime is 25 years; however, this does not consider variations in the space environment over time. Studies have shown a 10% variation in lifetime that generally cannot be accounted for in calculations [17]. Therefore, 25 years is treated as the maximum allowable lifetime, and the intended lifetime is

fixed at near 23 years in all calculations. The correction factor helps ensure that the spacecraft still deorbits within the 25-year limit, even in a worst-case scenario.

After the sail size is calculated, mass calculations for the required sails are performed. It is assumed that the material used in sail construction is constant in mass per unit area, with no additional considerations for design changes for larger sails. DeOrbitSail is used as a reference for the mass calculations, with the 25 m^2 sail being 3 kg [7]. This area-to-mass ratio, roughly 0.12 kg/m^2, is multiplied by the sail's size in m^2 to calculate the mass of the required drag sail for a 25-year deorbit for any given spacecraft. The solid lines in Figure 17 show the sail mass required to deorbit a CubeSat in no more than 25 years.

Drag sail mass must be compared to the required propellant masses to compare the effectiveness of the methods. Having solved the propellant mass to empty mass ratio in Figure 7 and knowing the mass of each CubeSat in the investigation, the mass required to dispose of a spacecraft using propulsive means can be calculated. Between the reentry trajectory and disposal orbit options, the reentry trajectory is the more efficient option at all altitudes below 1000 km. Figure 17 also shows the propellant mass required to deorbit a spacecraft for each CubeSat using traditional propulsive techniques, shown by the dashed lines.

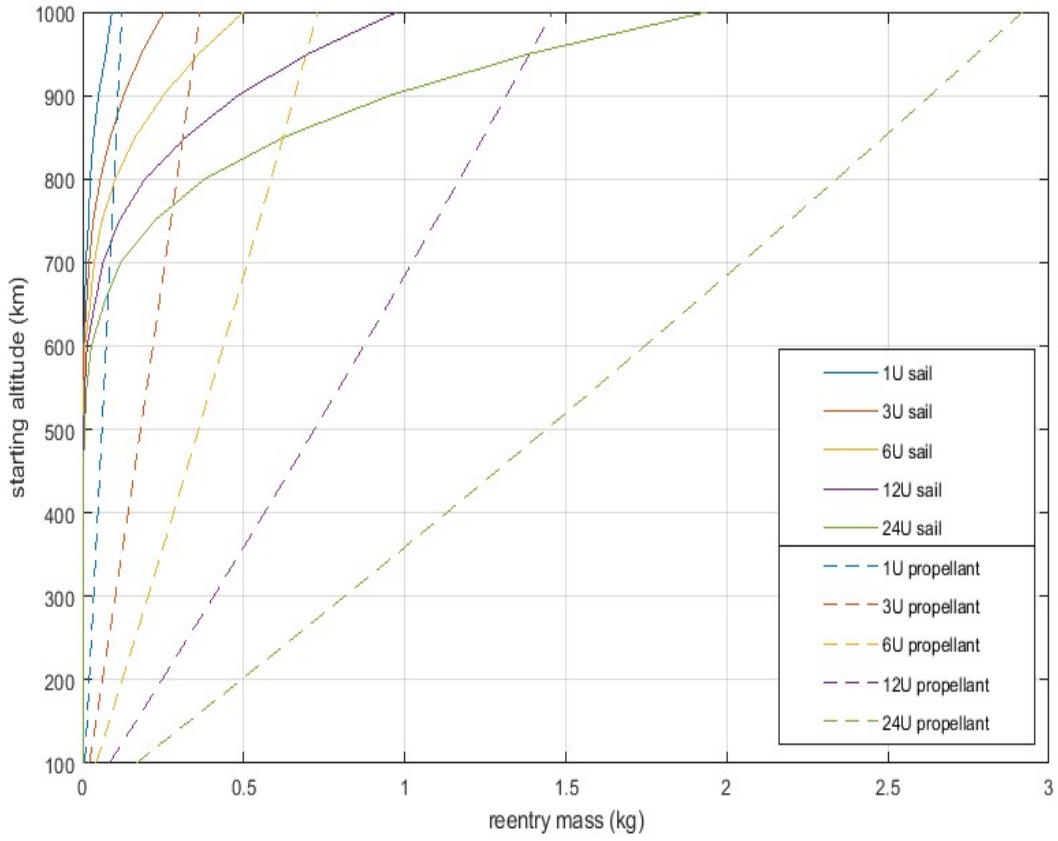

Figure 17. Sail and Propellant Mass Required for Targeted Reentry for CubeSats

The results of Figures 17 are then compared to gauge the result of the drag sail. The first noteworthy characteristic of the plots is the different shapes of the curves. Note, for the drag sail, that mass increases exponentially with altitude, while the propellant data is nearly linear for the studied altitude range. This factor highlights the differences in the lower altitudes, until about 500 km, as considering a drag sail is trivial because the CubeSats deorbit within 25 years regardless. As the altitude reaches the upper limit, values become more comparable. At 1000 km, the required deorbit mass is still lower for each CubeSat when the spacecraft is equipped with a drag sail instead of a propulsion system. The differences in values are not severe, with a 24U CubeSat requiring a 1.9 kg drag sail compared to 2.9 kg worth of propellant. The main result to

take away is that, for all CubeSat sizes, it would be more efficient to deorbit using a drag sail than to carry the required amount of propellant to deorbit. For reference, it costs about $10,000 to get a kg of mass launched into low-Earth orbit [3].

Large Spacecraft

The relative mass decrease of the CubeSat case suggests that further analysis of full-sized, operational satellites is warranted. Larger spacecraft do not have drastic changes in the area-to-mass ratios relative to CubeSats and require more substantial sail size modifications to create the same relative increases. Table 2 shows a representative sample of spacecraft types that may be found in low-Earth orbit, both current and former missions, and relevant properties associated with them [30].

The sample spacecraft were selected to show various types of missions performed in low-Earth orbit while representing the broad range of spacecraft sizes that could leverage sail-based deorbit technology. Also shown in the table are CubeSats that maintain a similar area-to-mass ratio as the larger spacecraft. The table shows that, despite the significant differences in mass, area-to-mass ratios remain within the same order of magnitude for different spacecraft classes.

Table 2. Low-Earth Orbit Spacecraft Examples and Properties

Type	**Name**	**Mass (kg)**	**Effective Area (m^2)**	**A/m (m^2/kg)**	**Comparative CubeSat**	**CubeSat's A/m (m^2/kg)**
Remote Sensing	ENVISAT	8211	18.75	0.0022835	24U	0.0027151
Earth Observation	ICESAT	1514	7.157	0.0047270	6U	0.0045948
Communications	Iridium	689	3.557	0.0051621	3U	0.0058480

Notice the broad range of spacecraft parameters for the representative sample. Iridium is a relatively small 689 kg, compared to ENVISAT with a mass of 8211 kg, several times the mass of an automobile. In this work, the scope will ensure that the drag sail can demonstrate a successful deorbit for an extensive range of spacecraft.

The three spacecraft were investigated similarly to the CubeSat configurations. The orbital lifetime was solved in each case, and the mass required to deorbit using a drag sail was found. Additionally, the propellant required to induce deorbit was evaluated. The values in each case were tabulated to compare cost savings by opting to deorbit using a drag sail instead of a propulsive reentry trajectory. Table 3 shows relevant information for the deorbit of the three spacecraft.

Table 3. Low-Earth Orbit Spacecraft Deorbit Times and Required Mass

	ENVISAT	ICESAT	Iridium
Altitude (km)	770	480	780
A/m (m^2/kg)	0.002284	0.004727	0.005162
Lifetime (years)	685.64	4.62	339.86
Propellant Mass Req (kg)	579.54	65.36	49.27
Sail Mass Req (kg)	67.89		6.38
Sail Size Req (m^2)	565.72		44.79
Sail Side Length (m)	23.78		7.294

For the three cases considered, two spacecraft are relevant cases in that they do not deorbit in under 25 years without a drag sail. ICESAT orbits at a lower altitude than the other two; thus, the spacecraft would not take 25 years to deorbit regardless of configuration. The other two spacecraft would deorbit in a few hundred years, making them relevant to this study. Consider the required propellant mass compared to the mass of a drag sail required to deorbit in under 25 years. For both the ENVISAT and Iridium cases, the mass required for propulsive entry is close to 10 times the mass of the sail that would be leveraged for deorbit. The preliminary results indicate that adding a drag sail is a promising solution to a deorbit strategy. Significant mass reductions may be possible by implementing a drag sail instead of strictly relying on propulsive techniques to perform end-of-life operations. The one potential apparent setback at

this point is the size of the sails that would be required for a successful deorbit. DeOrbitSail was proposed as a 5 m x 5 m sail, and the requirements for a sail to deorbit ENVISAT or Iridium would significantly expand on the current technology. Iridium required a 7.3 m x 7.3 m sail, which may be feasible given its proximity in size to DeOrbitSail. However, the 24 m x 24 m sail required to deorbit ENVISAT would need significant technological advancements. The largest sail ever designed for space was NASA's Sunjammer, which boasted a 38 m x 38 m sail, substantially larger than a sail required for ENVISAT [31]. However, Sunjammer was never deployed in space, making it an untested technology. Additional validation of the technology would be necessary to advance the concept. Moreover, Sunjammer was designed as a solar sail, not a drag sail. A sail would experience significantly larger drag forces in close proximity to Earth than a sail on an interplanetary trajectory, made evident from Figure 8. Additional structural considerations to design a drag sail capable of withstanding higher forces are required.

In the subsequent section, larger spacecraft with masses ranging from 1000 kg to 7000 kg are investigated. Nonetheless, the area-to-mass ratios are on the same order of magnitude as the CubeSats data in Table 2. Recall that Figure 15 shows the expected lifetimes for spacecraft, with many exceeding 1000 years. However, only altitude and mass play a role when considering mass requirements with a given set of assumptions. In this investigation, the frontal area is evaluated to deorbit a spacecraft in 25 years. The results in Figure 18 show the propellant mass required for spacecraft with a given empty mass to perform a targeted reentry using a traditional propulsion strategy. The trends are similar to those in Figure 17. The required propellant mass is a function of the empty spacecraft mass only, apparent from Equation 9; as the spacecraft sizes increase, the propellant required also increases. With the larger spacecraft, masses for reentry become exceedingly significant, often requiring several hundred kilograms of propellant to reenter.

Next, a comparison is made to deorbit a spacecraft using a drag sail. The same process can be used to find the sail mass as the CubeSat analysis. Figure 18 shows the drag sail mass required for spacecraft reentry from specific altitudes as solid lines. Comparing the two sets of data in Figure 18, the goal of minimizing the end-of-life mass requirements for a mission, this study overwhelmingly supports the use of a drag sail. Even at higher altitudes, propulsive reentry requires at least 50% more mass than a drag sail. Given the exponential nature of the drag sail compared to the near-linear nature of the propellant, at lower altitudes the mass discrepancy is even greater. With ongoing technological advancement, the data suggests that reentry using a drag sail is far more efficient than implementing a propulsive reentry.

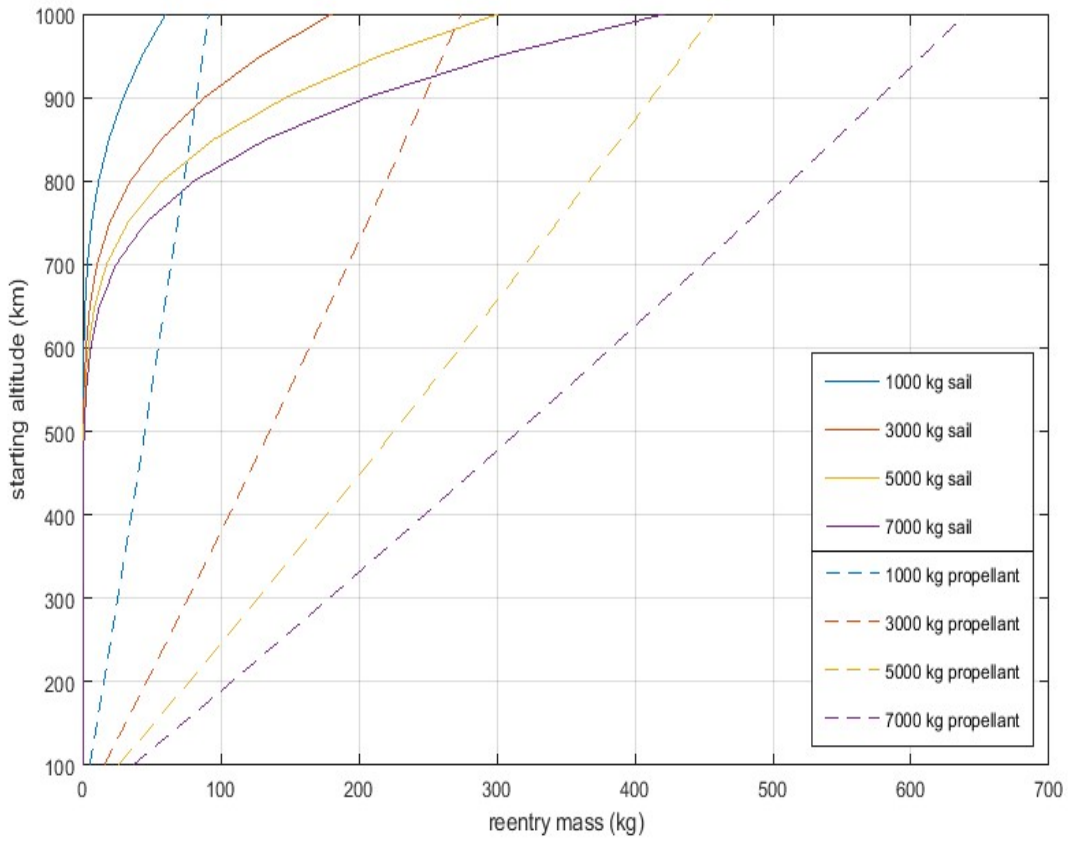

Figure 18. Drag Sail and Propellant Reentry Mass for 25-year Deorbit of Large Spacecraft

Despite the promising preliminary deorbit analysis, it is unclear whether the current technology can support drag sail size requirements. ENVISAT initially brought into question specific issues with sail construction, and this study expands on the same concerns. Analyzing the data on generalized large spacecraft, significant sail sizes would be needed in some cases, potentially even larger than those considered for ENVISAT. No spacecraft larger than ENVISAT are investigated in this study, representing a reasonable threshold as larger spacecraft are often space stations or other manned platforms [30]. It is conceivable that a larger spacecraft could benefit from a drag sail application; however, it is yet to be fully explored. Figure 19 shows the sail areas required to deorbit spacecraft from various altitudes.

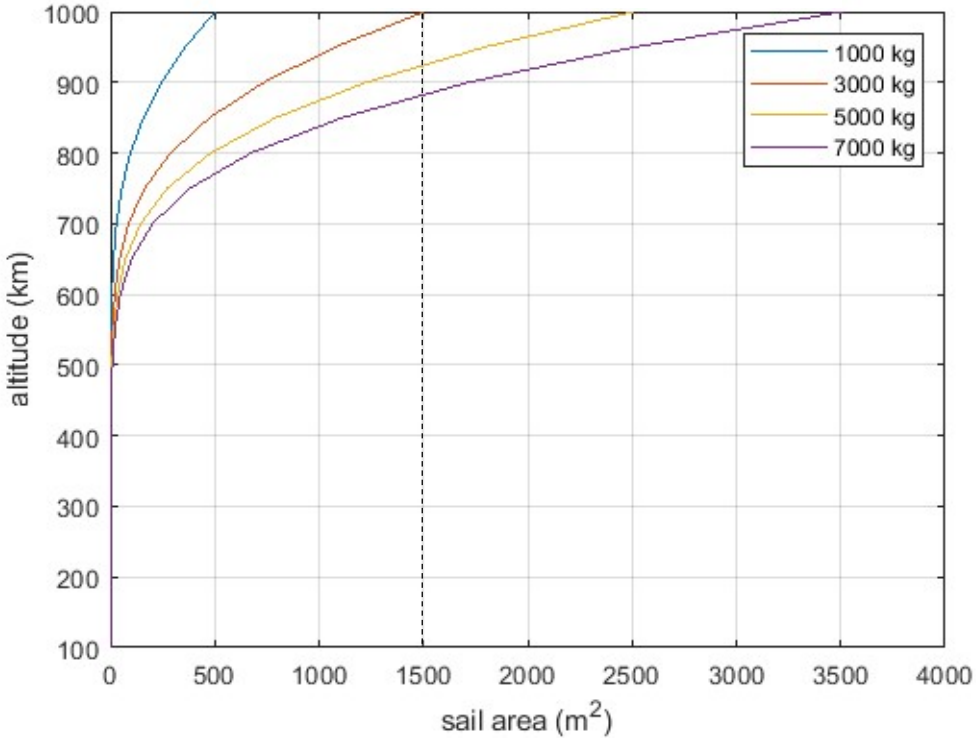

Figure 19. Drag Sail Area Required for 25-year Max Reentry Time

For large spacecraft, sail sizes much greater than the 25 m^2 DeOrbitSail are generally observed. For a 7000 kg spacecraft at 1000 km, the sail would be nearly 60 m x 60 m. Even at the same altitude for a 1000 kg spacecraft, the sail would need to be 22 m x 22 m. It is unclear whether this requirement is technologically feasible at this moment. The vertical, dashed line at 1500 m^2 is the absolute threshold of the current technology based on Sunjammer. Most of the data in Figure 19 is below the threshold set by Sunjammer, giving a large number of potential options to consider. Regardless, this investigation suggests that using a drag sail to deorbit is an effective and efficient way to complete spacecraft end-of-life operations, given additional drag sail testing.

Extended Perturbation Analysis

Having analyzed the simplified version of lifetime calculation, direct numerical integration can be pursued further. Using numerical integration limits the amount of data that can be considered quickly; however, it is required for a broader analysis of specific parameters. The focus of this section is to analyze the effects of other perturbations on the orbit and validate the prior assumptions, both for spacecraft with and without drag sails. For this investigation, MATLAB's built-in ODE45 solver was used for all integration, with tolerances of 10^{-12}.

To make an effective comparison, two situations are considered. First, a 24U CubeSat with no sail is analyzed to deorbit a spacecraft from 500 km. Second, a 25 m^2 sail is implemented on the CubeSat and propagated from 950 km. The altitude difference intends to match the total lifetime between the two scenarios. Within those two configurations, the perturbations are first analyzed separately, then all together. Drag and J_2 are processed together initially due to the forces acting in a single direction of the orbit, and then SRP is analyzed separately to draw conclusions on its effects.

Perturbations on a CubeSat: No Sail

The first study was performed by propagating the 24U CubeSat from a 500 km altitude near-circular orbit. All other orbital elements were selected as representations of what may be exhibited in a low-Earth orbit. The orbit is inclined at 30°, with an argument of perigee of 60°, right ascension of the ascending node of 40°, and true anomaly of 30°. Note, certain orbital elements become undefined when eccentricity equals zero, so the propagator accounts for a small, finite value on the order of 10^{-4}. The propagator continues to use a gravitational model with Earth defined as a point mass. Figure 20 shows the change in altitude throughout the spacecraft's lifetime. The final value is about 11.4 years, with the simulation concluding when the spacecraft reaches the previously used 86 km threshold, implying that it has successfully deorbited. Also, note the exponential nature of the data is due to the significant increase in atmospheric density as the altitude decreases.

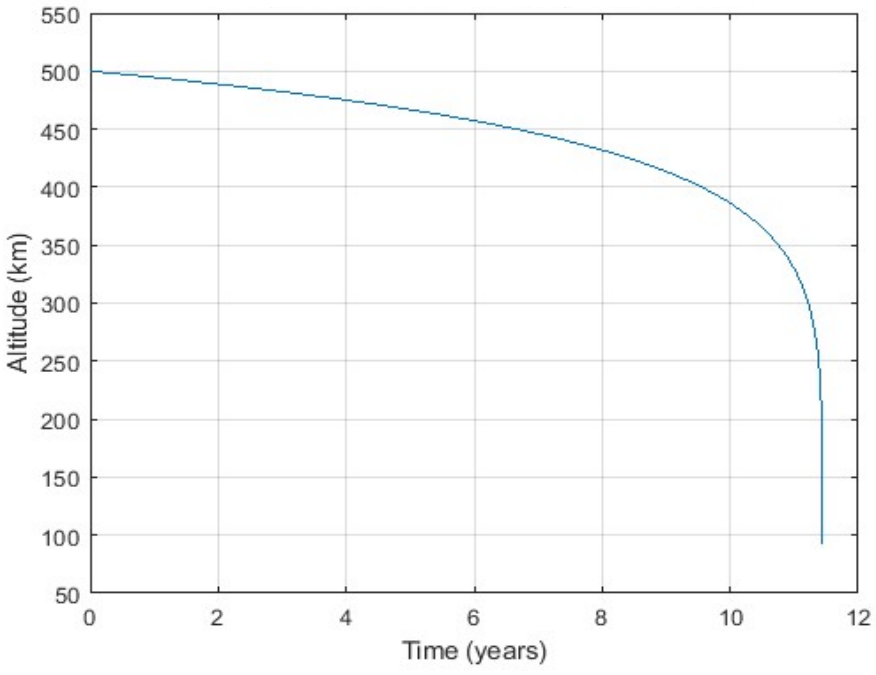

Figure 20. Effects of Atmospheric Drag on 24U CubeSat Lifetime

Isolating drag results in the spacecraft deorbiting over time, but SRP should not have this effect on its own. Drag acts exclusively opposite the velocity vector, whereas the Sun is viewing the spacecraft from a different angle at each instant. Figure 21 shows the effects of solar radiation pressure on the altitude and eccentricity of the spacecraft's orbit. In Figure 21b, the altitude oscillates but shows nearly no change over the 25-year propagation. Note, the altitude plot is not centered around 500 km. The non-zero eccentricity makes it so the starting altitude is closer to 500.0005 km. Although solar radiation is a significant force in terms of magnitude, it oscillates with each sidereal day for over 4000 days, so the change is insignificant relative to its initial state in the long term. The changes make it apparent that, in this case, SRP causes an insignificant change in altitude. Specifically, note the trend of the oscillations. Two peaks and two troughs occur every year due to the seasonal changes of the orbit. CubeSats have a small area-to-mass ratio (approximately 0.0027 m^2/kg for 24U), which contributes to the minimal perturbation caused by solar radiation. However, the area-to-mass ratio would also be a factor when considering drag, so the relative significance requires further investigation.

Now consider the effect of eccentricity on the orbit. The trend of the eccentricity changes very little over the 25 years, 6.5×10^{-5} on average, but it oscillates every year, per Figure 21a. The oscillations are likely due to the rotation of the force around the spacecraft the Sun provides as it rotates around in the spacecraft-relative frame. On one side of the orbit, the Sun is more likely to act from behind the spacecraft, increasing its eccentricity. On the other side, the Sun is in the front, decreasing the eccentricity. Refer back to Figure 10 for a visualization. The phenomenon also explains the effects on the altitude. Unlike altitude, the average value of eccentricity noticeably increases over the 25-year propagation. The change is a relatively significant amount, although the magnitude is still rather small. However, Figure 21b shows that the solar radiation

pressure has minimal impact on the orbit for the given case. The same negligible impact became apparent as when orbits at different altitudes were investigated in the propagator.

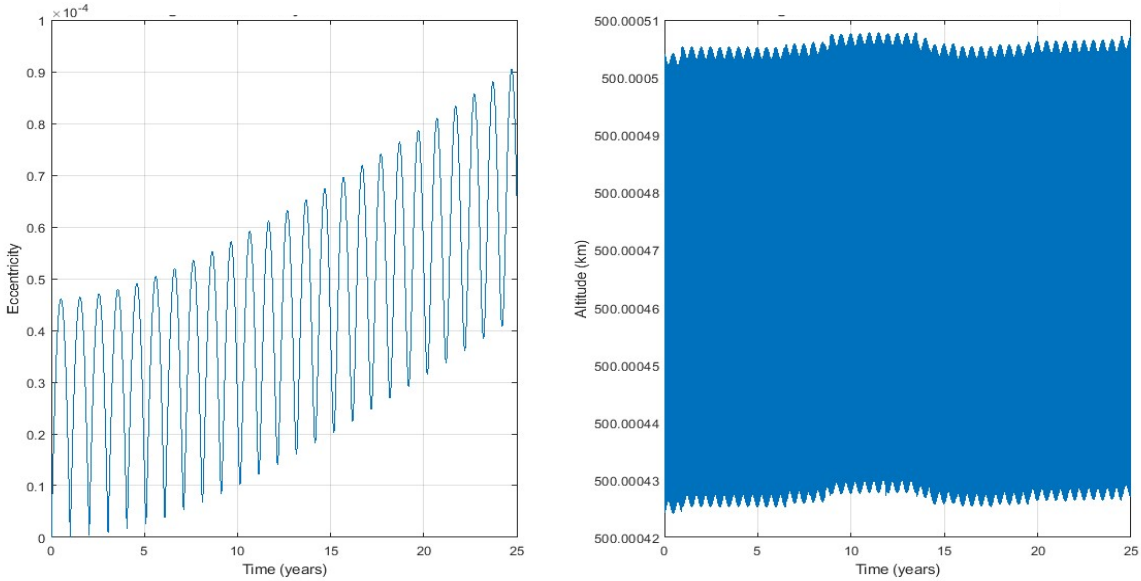

a) Eccentricity vs. Time **b) Altitude vs. Time**

Figure 21. Changes in Eccentricity and Altitude from SRP on a 24U CubeSat at 500 km

To further continue the analysis, both drag and SRP perturbations are incorporated in the dynamical model. Refer back to Figure 20 for the lifetime plot, as the data does not change between the two scenarios. Given Figure 21, it is apparent that solar radiation does not significantly modify the trajectory relative to the drag force on the spacecraft. The lifetime of the spacecraft remains at 11.4 years, with no notable change to lifetime. Figure 22 shows the orbital elements throughout the spacecraft's lifetime, including inclination, right ascension of the ascending node, and argument of perigee. The additional orbital elements have minimal variation over the spacecraft's lifetime. Inclination changes are negligible, on the order of 10^{-8}, shown in Figure 22b. Eccentricity oscillates in the same way as the SRP-only model; however, no increase is noted in this situation, as Figure 22a suggests. The argument of perigee and right ascension of

the ascending node oscillate between 0° and 360° over the lifetime, which can be attributed to the drift caused by J_2 effects, apparent in Equations 37 and 38. The changes over time for argument of perigee and right ascension of the ascending node are shown in Figures 24c and 24d, respectively.

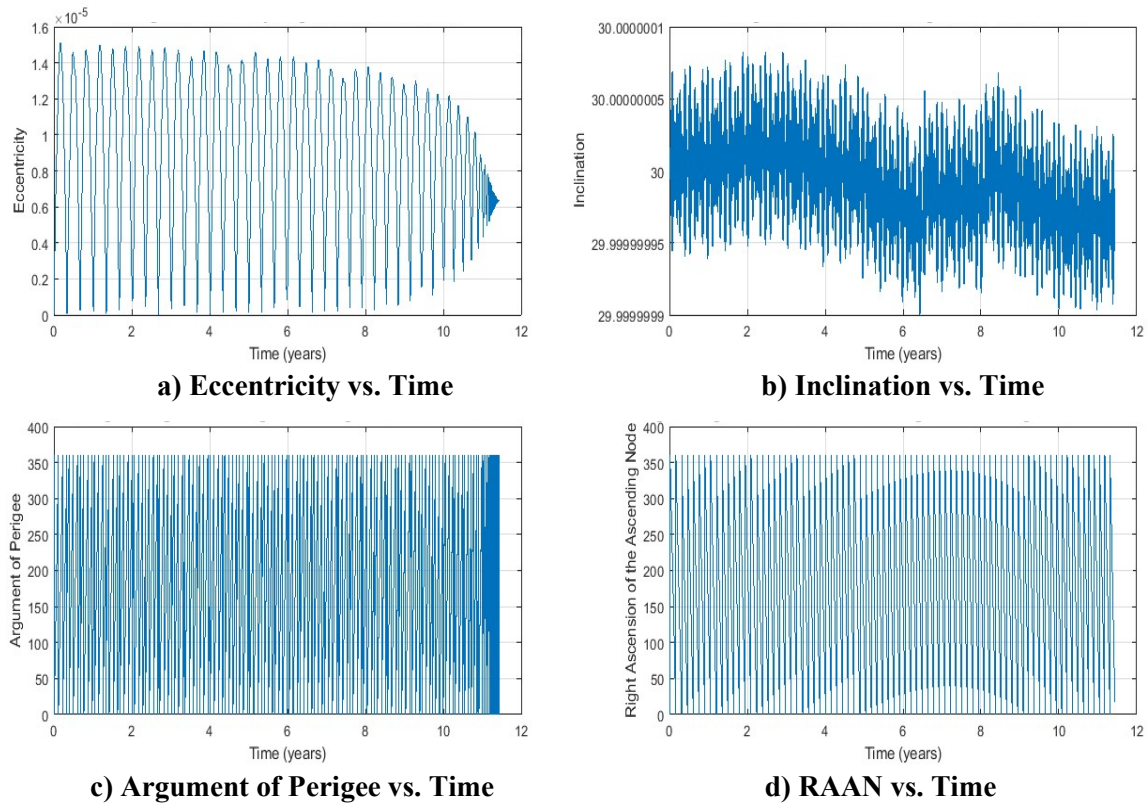

a) Eccentricity vs. Time

b) Inclination vs. Time

c) Argument of Perigee vs. Time

d) RAAN vs. Time

Figure 22. 24U: Orbital Element changes from Drag and SRP

The result of SRP is relevant for the analysis of long-term trends of lifetime data. Given the information, it is reasonable to assume that when analyzing the lifetime of low area-to-mass ratio spacecraft, the effects of solar radiation pressure can be considered negligible. It was noted in Figure 8 that at near 625 km, solar radiation pressure becomes the predominant force; hence additional analysis is required to make assumptions for significant increases in altitude.

Perturbations on a CubeSat: 25 m^2 Sail

Having considered the default CubeSat configuration, the next step is to add a drag sail to the spacecraft. A 25 m^2 sail is used based on DeOrbitSail. A brief analysis of the standard CubeSat parameters shows that a few changes need to be made. Notably, a 25 m^2 sail on a 24U CubeSat deployed from 500 km causes the spacecraft to deorbit in approximately two weeks, which does not offer enough time to fully quantify the differences between drag and SRP perturbations on the spacecraft. Thus, the altitude is raised to 950 km, thereby increasing the sail-based spacecraft's lifetime and thoroughly analyze the result of the effects of SRP and atmospheric drag on the deorbit strategy. Specifically, 950 km is selected to achieve a similar total lifetime value to the sail-less scenario.

Similar to the default 24U CubeSat, the first step is to consider an orbit perturbed only by atmospheric drag. The numerical integration process for propagation is the same as the previous scenario with updated parameters for spacecraft frontal area and altitude. The resulting plot is shown in Figure 23. The trend is consistent with the previously shown Figure 20, with an exponential decline in altitude, leading to the spacecraft's eventual deorbit. The new scenario takes 10.6 years (3,857.9 days) for the spacecraft to be deorbited. The time falls well within the NASA 25-year limit, which would have been significantly exceeded had a sail not been implemented. Expected deorbit times for a spacecraft with a similar size from 950 km altitude were shown to be on the order of 1000 years in Figure 15.

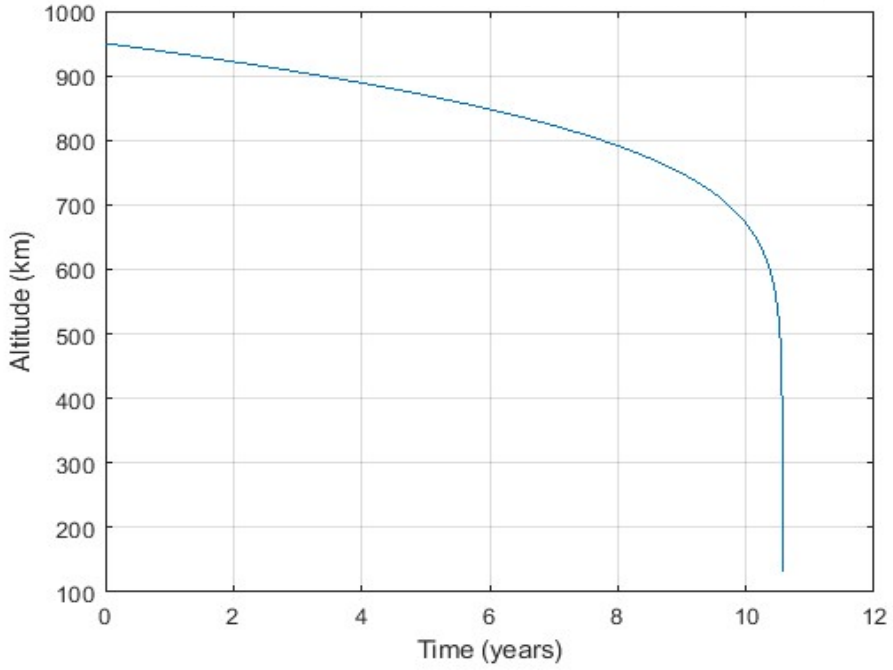

Figure 23. Effects of Atmospheric Drag on Lifetime of a 24U CubeSat with Sail

The data from the drag-exclusive case reflects the trend seen for the low area-to-mass ratio spacecraft. From here, SRP can be implemented. Figure 24 shows the eccentricity and altitude changes over a 25-year orbit propagation. For eccentricity, in Figure 24a, the data trend follows very closely to the behavior of the sail-less spacecraft. The scale of the changes is significantly higher, about three orders of magnitude compared to the prior case, but the general trend remains unchanged. As with previous examples, notice the oscillations taking place every year due to the Earth's rotation around the Sun.

However, the altitude shows a much different trend than that of the sail-less model, comparing Figure 24 to Figure 21. The primary outcome from Figure 20 was that there were no meaningful changes to the elements due to the spacecraft maintaining nearly the same altitude for the entirety of the propagation. However, when a sail is incorporated, the altitude makes noticeable changes throughout the propagation. Over the 25 years, the SRP consistently increases

the altitude of the orbit. The magnitude remains small; however, it becomes clear that SRP can potentially induce changes to the orbit when a drag sail is implemented.

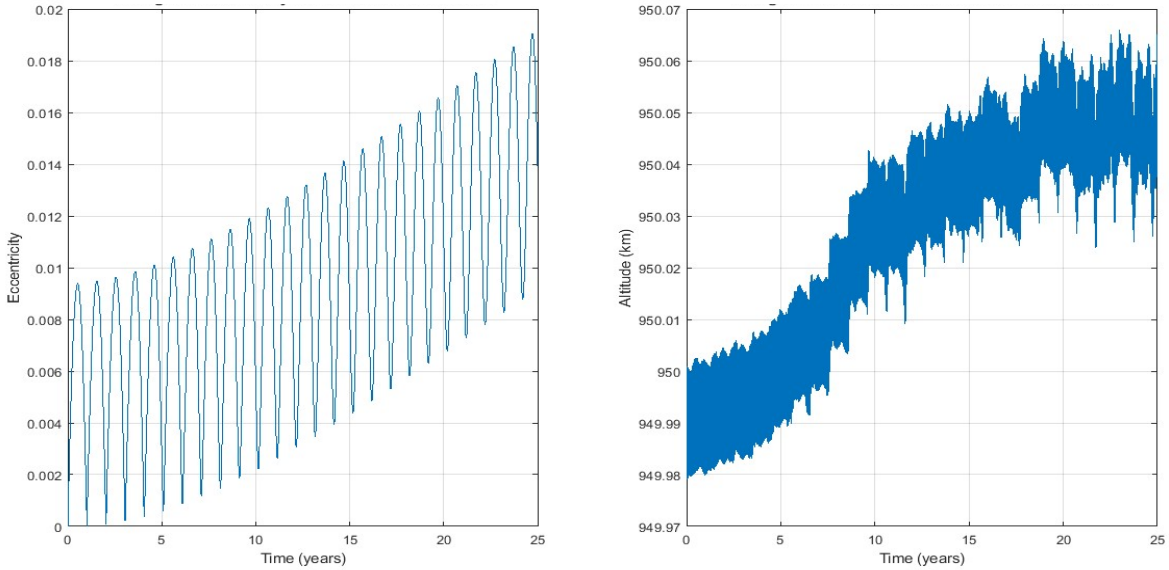

a) Eccentricity vs. Time **b) Altitude vs. Time**

Figure 24. Changes in Eccentricity and Altitude from SRP on a 24U with a Sail at 500 km

Given the noticeable increasing trend in altitude from the solar radiation pressure, it is conceivable that the total lifetime of a spacecraft is affected by SRP at a higher area-to-mass ratio relative to the initial case. Like the standard CubeSat study, drag and solar radiation pressure forces are implemented together into a singular orbit simulation. Figure 25 shows the total lifetime of the 24U CubeSat equipped with a 25 m^2 drag sail deployed at end-of-life from 950 km.

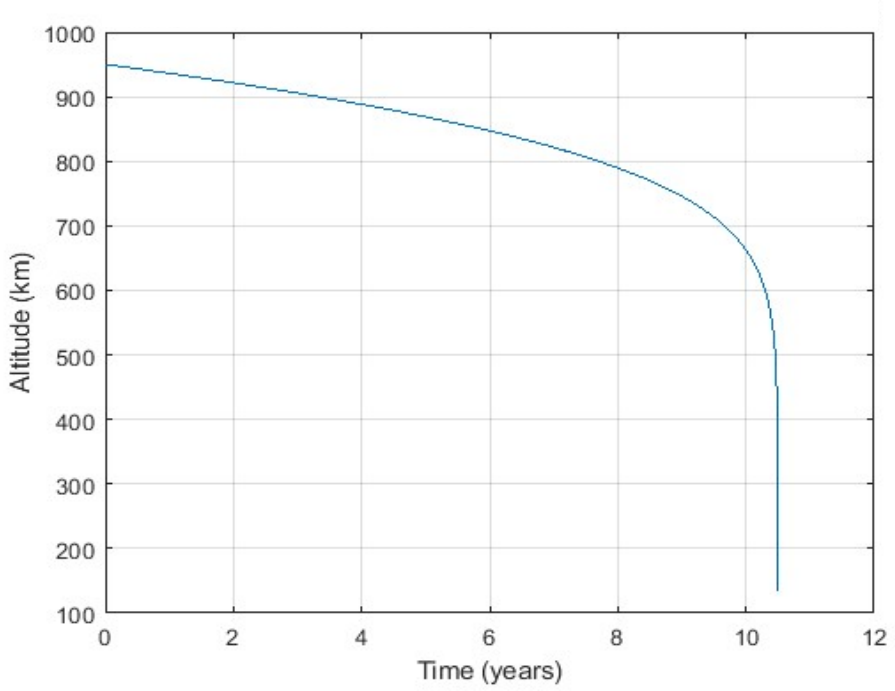

Figure 25. Effects of Atmospheric Drag and SRP on Lifetime of a 24U CubeSat with Sail

Next, compare Figure 25 with Figure 23. Unlike the scenario investigated without a sail, there is a difference in the lifetimes. By implementing SRP, the lifetime decreases to 3831.1 days, a 27-day decrease. However small, this suggests that solar radiation pressure can be leveraged to decrease the total lifetime further than merely relying on atmospheric drag at sufficiently high area-to-mass ratios.

Figure 26 shows the changes in the other orbital elements over the spacecraft's lifetime as a result of the incorporated drag sail. The right ascension of the ascending node and argument of perigee in Figures 26c and 26d do not change, primarily because J_2 is still the main driver of changes to those elements. The other elements in Figures 26a and 26b are orders of magnitude different between the two cases. Inclination remains relatively unchanged, although the four orders of magnitude difference reflects the effect of SRP. The lack of overall change is likely because the Sun does not exert significant out-of-plane force on the spacecraft, especially at low

inclinations. Eccentricity follows a similar trend but with larger changes in magnitude. As with the previous scenario, the positive trend observed in the SRP-only case is no longer present, with the average being near-constant throughout the lifetime. The more apparent changes in the orbital elements are likely due to the increased area-to-mass ratio. Drag does not play a significant role at higher altitudes, and the Sun is the primary driver of the changes in the orbital elements. It was apparent in the previous case that the smaller spacecraft could not leverage the force from the Sun to change lifetime. When the sail was implemented, the SRP from the Sun played a critical role on the spacecraft and significantly changed the orbital elements.

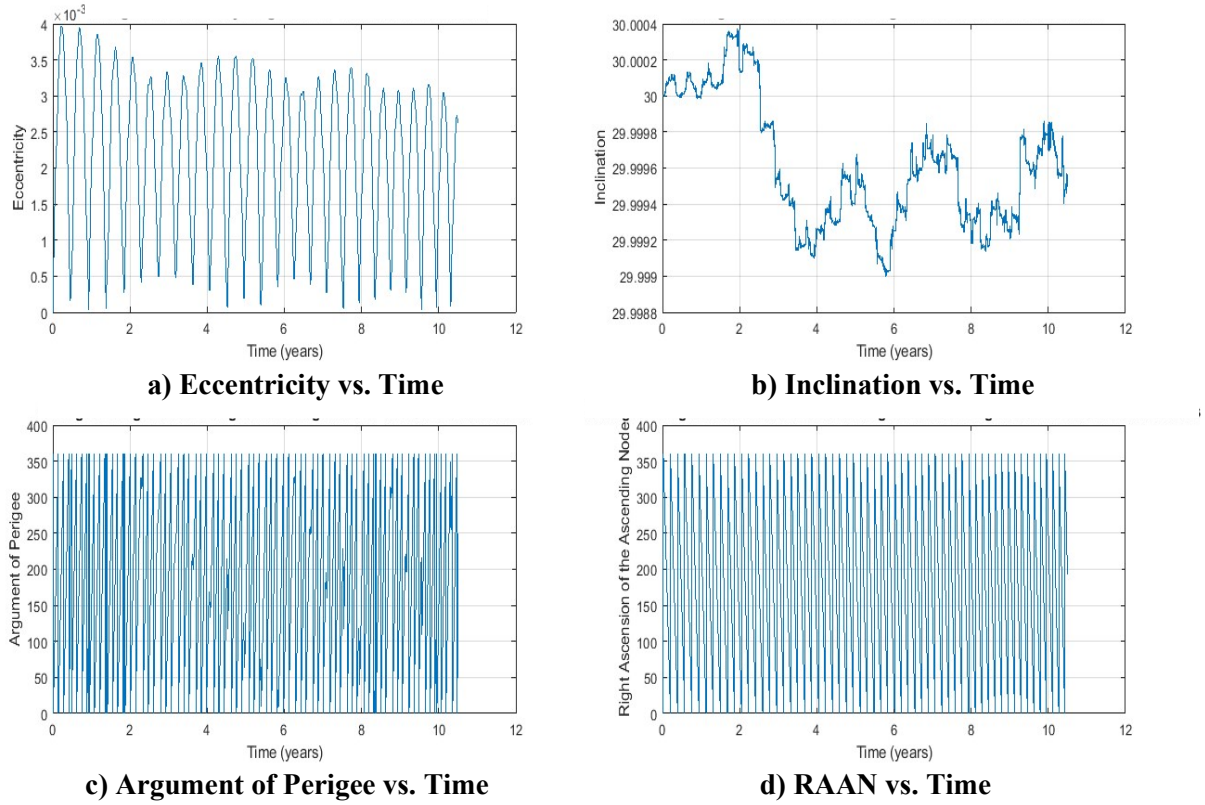

a) Eccentricity vs. Time

b) Inclination vs. Time

c) Argument of Perigee vs. Time

d) RAAN vs. Time

Figure 26. 24U with Sail: Orbital Elements Changes from Drag and SRP

Comparing the two forces due to atmospheric drag and solar radiation pressure, it is apparent that the drag force has a significant effect on the overall trajectory and lifetime. Solar radiation pressure plays an additional role; however, it is significantly less in effect, especially at lower altitudes. The analysis presented shows that the area-to-mass ratio is a primary factor for changing the impact of solar radiation on the propagation. The effect may be worthy of further investigation since any decrease in lifetime that results from leveraging the Sun is a step towards optimizing the process of accelerated spacecraft deorbit. In the scenarios presented, however, the overall change resulting from the implementation of SRP is minimal to the point where a drag-only assumption would be viable. Given that the change in lifetime is negative, any decrease in lifetime provided by the sail and solar radiation effects would be an acceptable factor of safety and does not negatively affect estimates.

Effects of Eclipse

The preliminary analysis using the orbit propagator was performed with the assumption that SRP is always acting on the spacecraft. The assumption considers the spacecraft attitude, meaning the force of the Sun is not constant throughout the orbit despite always acting to some extent. The model simplified the analysis; however, it does not represent the precise effects of SRP on spacecraft as it moves along its trajectory. Incorporating the effects of a spacecraft's presence in eclipse can be simulated propagating the same orbit region with the binary shadow function, ν, as a variable. Equation 26 and Figure 10 shows how the change would affect the scenario. Figure 10 suggests that the time in which the spacecraft is in eclipse is the time that the sail is nearest to parallel of the Sun's rays. In addition, the perturbation force of SRP acts radially to the orbit's path at this point, meaning that the magnitude of the velocity change is small relative to other points in the orbit, which can be seen by applying Equation 8. These two factors

suggest that whether the spacecraft is subject to eclipse is inconsequential to determining the spacecraft's total lifetime due to the minimal ΔV imparted on the spacecraft in its orientation.

The two prior scenarios analyzed, 24U CubeSats with and without drag sails, were propagated again in a model that considers the effects of eclipses on the spacecraft by the Earth. Neither case reflects more than a fraction of a day difference compared to the initial case with no eclipse. Visually, Figures 20 and 25 sufficiently display the data of the new case. Given this, it is reasonable to propagate the orbit with the Sun treated as always on. As far as the spacecraft operation goes, knowing these periods of eclipse is essential. However, strictly for projecting lifetime, this factor is inconsequential in this investigation.

Eccentric Orbits

Thus far, spacecraft were assumed to be in circular orbits. To increase the fidelity of the analysis and test the effects on non-circular orbits, spacecraft situated in eccentric orbits must be briefly considered. Consider a 24U CubeSat example in an orbit with a 950 km apogee and perigee of 300 km. The change results in an orbit eccentricity of 0.046. The propagation method dictated by Equations 13-18 and the initial spacecraft state remains the same, and SRP is turned off for this example, as suggested in the discussion on eclipse. Comparative scenarios of eccentric orbits show similar results of SRP as the circular orbit. Figure 27 shows an altitude vs. lifetime plot for this scenario. Note that the value of altitude referenced is the average altitude, which refers to the semi-major axis minus the Earth's radius.

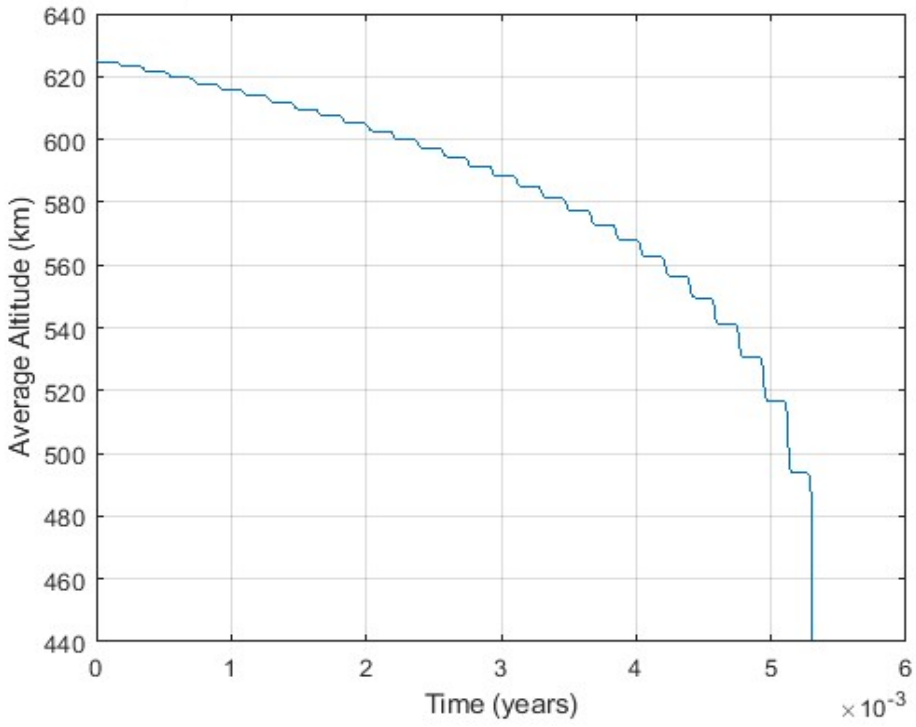

Figure 27. 24U CubeSat with Sail Lifetime for an Eccentric Orbit, e=0.05

Compared to the altitude vs. time plots for the circular orbits in Figures 20 and 25, there are very distinct steps in each orbit apparent in Figure 27. The atmospheric density is significantly greater at the 300 km perigee than 950 km apogee, despite the relatively low eccentricity of the orbit. Per Figure 4, the change in atmospheric density is over three orders of magnitude. As a result, the majority of the decrease in altitude occurs when the spacecraft is near perigee. This behavior explains the apparent steps in Figure 27, where the altitude does not significantly change when the spacecraft is near apogee due to the low atmospheric density and rapidly decreases in altitude near perigee.

Next, consider the spacecraft lifetime shown in Figure 27. It is clear that the decrease in perigee significantly decreases the lifetime. The 10-year plus circular orbit in Figure 25 decreases to only a few days due to the increased drag force acting on the spacecraft near

perigee. Referring back to the eccentric orbit estimates in Figure 16, the order of magnitude expected by these parameters matches the estimated value for lifetime.

For the eccentric orbit case, there are no unexpected results. It had been shown that an eccentric orbit decreases the lifetime of the spacecraft compared to circular orbits with similar semi-major axes, and the investigation validates that. The example with the 24U CubeSat in an orbit with 0.05 eccentricity, given the similar results to the previously used effective altitude method dictated by Equation 5, confirms the results seen in Figure 16. For specific lifetime examples for spacecraft in eccentric orbits, the numerically integrated propagator is the preferred method if broad data trends are not required.

Comparison of Drag and SRP

Having observed the effects of the perturbations due to atmospheric drag, SRP, and J_2, it is critical to compare the magnitude of the forces acting on the sail-based spacecraft due to each perturbation. SRP and drag are exclusively considered given that J_2 does not exert a force on the spacecraft that changes the energy of the orbit per the discussion about Equations 37 and 38. Now, consider another 24U CubeSat equipped with a drag sail and deployed from an altitude of 800 km. Over the CubeSat's lifetime, the acceleration of the atmospheric drag and SRP perturbations are taken at each time step. The comparison takes eclipse times into account; thus, SRP is inactive when the spacecraft is in Earth's shadow. The periods of eclipse are not visible in the results because they are too frequent and too short to be represented at this scale. The results are shown in Figure 28.

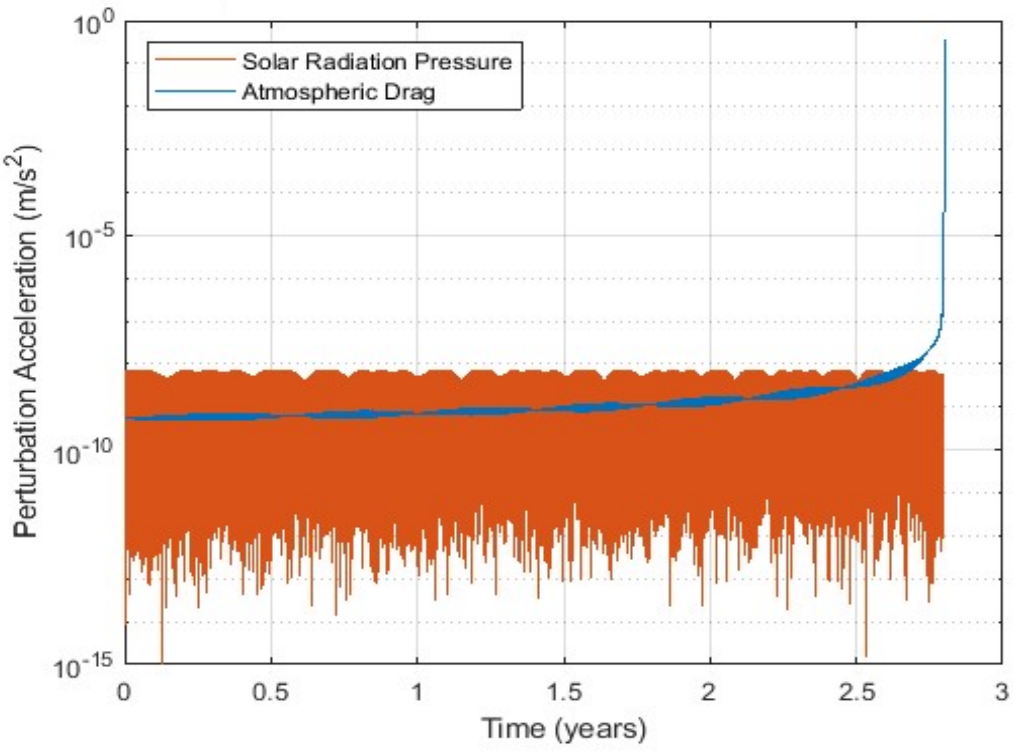

Figure 28. Difference in Perturbations over Time: 24U CubeSat with Sail, 800 km

To understand and compare the variation of the perturbing forces due to the change in altitude, another representation of the perturbations over the lifetime is shown in Figure 29. Figures 28 and 29 show the same scenario for a 24U CubeSat with a drag sail and an initial altitude of 800 km. The plot in Figure 29 helps visualize the differences in the magnitude of the perturbations relative to the altitude instead of time.

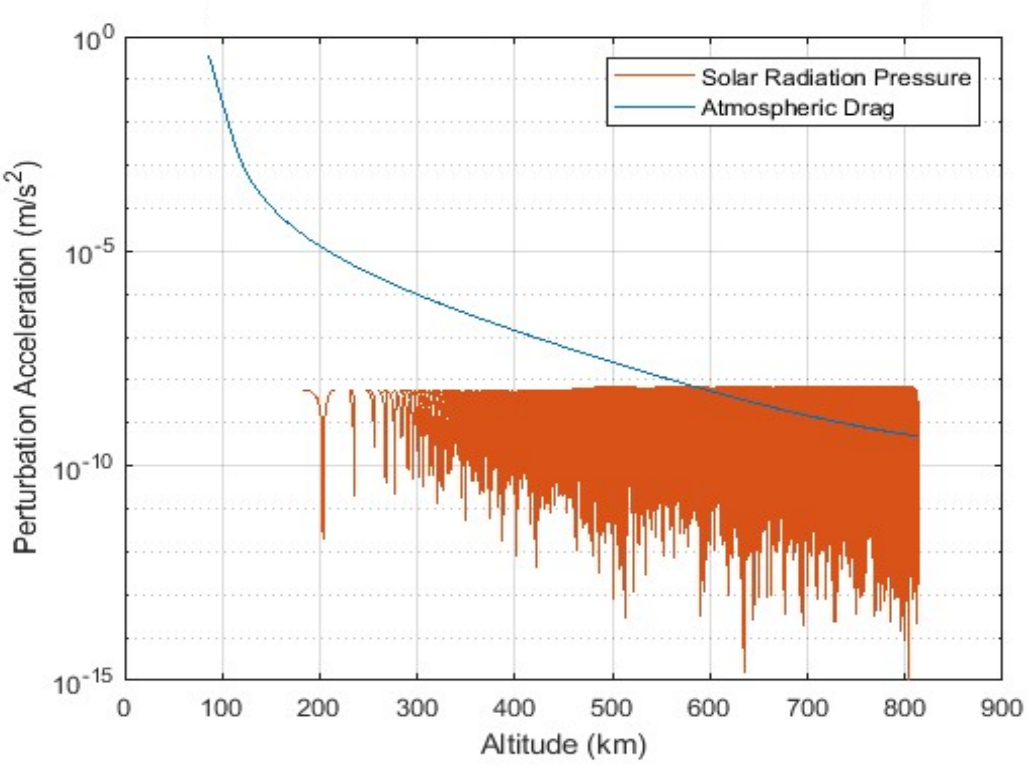

Figure 29. Difference in Perturbations over Altitudes: 24U CubeSat with Sail, 800 km

The effect of atmospheric drag on spacecraft lifetime calculations shows exponential growth as the spacecraft nears the Earth, according to Figure 29. The majority of the increase occurs near the end of the lifetime from a time standpoint, per Figure 28. A reason for the discrepancy is that the two primary determiners of the drag force in Equation 2, atmospheric density and spacecraft velocity, do not change proportionally to each other. Velocity increases by a few hundred meters per second throughout low-Earth orbit, while the density changes by eight orders of magnitude between 900 km to 100 km. The discrepancy causes the perturbation to increase more drastically at lower altitudes. Solar radiation pressure does not have the same rapid change in magnitude; however, it undergoes consistent change throughout the spacecraft's lifetime. The average maximum value remains near $1x10^{-8}$ throughout, but the actual value varies substantially. The reason for the momentary changes in SRP force is the changing attitude

of the spacecraft, with the sail rarely oriented normal to the Sun. Although the maximum is significantly greater than the starting magnitude of drag, approximately $1x10^{-10}$, the average value is closer to drag. Given that the SRP is not acting consistently in a single direction like drag is, it becomes clear why drag has a much more significant impact on the orbits than SRP.

Now compare Figures 28 and 29 for the differences in time and altitude. Expressing the same orbit with two different x-axis variables shows a few distinct trends. Note that in Figure 28, the orbit trajectory only continues for a small fraction of a year once the atmospheric drag exceeds the maximum SRP perturbation. Compare this to Figure 29, in which the majority of the altitude range shows atmospheric drag exceeding SRP. The comparison shows that the satellite spends most of its orbital lifetime at higher altitudes. Even in the absence of SRP, the sharp increase in atmospheric drag results in a drastic decrease in altitude, causing accelerated reentry. Setting the Equations 21 and 26 to be equal, the point of intersection occurs at 584 km. The altitude value at which the magnitude of the drag perturbation matches that of SRP is different than the 625 km altitude shown in Figure 6. The altitude difference can be attributed to the difference in parameters used in calculating each perturbation and the time dependency displayed by the acceleration.

Targeted Reentry

The final set of results concerns the application of targeted reentry procedures to the orbital lifetime work. Initially, the altitudes from which targeted reentry can be achieved are discussed, followed by a few scenarios of location targeting. Like the prior sections, CubeSats are discussed initially, followed by some discussion on the ramifications of applying the process to larger spacecraft.

Maximum Altitudes for CubeSats

To successfully apply the targeted reentry method, both the maximum altitude for a longitude range and specific location targeting must be considered. The analysis is performed with CubeSats of four sizes: 3U, 6U, 12U, and 24U. The 1U case is ignored in this study, given that the 25 m^2 sail may not be applicable to the CubeSat, as well as the short reentry times observed at the area-to-mass ratios for this configuration, shown in Figure 15. The primary interest is CubeSats equipped with drag sails; however, it is essential to consider the scenario without drag sails for comparison. Given the passive nature of the studied targeting process, there is no difference in the method of analysis for CubeSats without drag sails.

The results of the numerical integration analysis show that the impact of SRP on lifetime calculations is insignificant in Figures 20-26. Thus, atmospheric drag is the only perturbation considered in this section. The method for solving for lifetime by integrating Equation 4 is used, given that no changes were noted from the numerical integration of Equations 13-18. The calculations allow for the analysis of trends for larger data samples not practical with numerical integration due to time constraints.

The initial step of the targeted reentry process is to determine the maximum total deorbit time a spacecraft can undertake while achieving reentry in a particular longitude range. The deorbit time is a constant for all spacecraft attempting to maintain a certain longitude range for given initial conditions and configurations. Figure 30 shows the maximum deorbit time vs. safe reentry range, assuming a 10% random variation in deorbit times. Note, the deorbit times shown are the maximum times, so a shorter deorbit in a specific scenario will positively affect the safety ramifications of the mission in terms of minimizing the chance of impact to objects on Earth's surface.

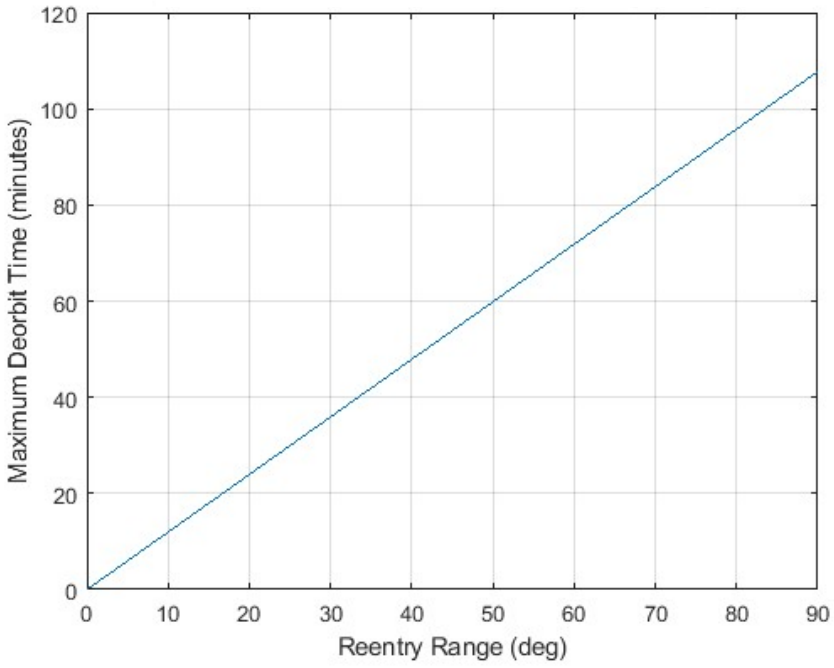

Figure 30. Maximum Reentry Time for a Specific Reentry Corridor

From Figure 30, note the near-linear relationship between the values. For all situations within the previously discussed 90° limit, the time to deorbit from the starting point must be less than two hours. The time may be less for more specific targeted locations, for example, approximately 10 minutes for a 10° reentry corridor. Table 4 shows reentry corridor lengths in terms of degrees longitude, with more accurate times to deorbit a spacecraft.

Table 4. Maximum Reentry Time for Specific Reentry Corridors

Reentry Corridor (°)	15	30	45	60	90
Maximum Time (minutes)	17.96	35.92	53.88	71.83	107.75

The values in Table 4, ranging from 18 minutes to 1 hour 48 minutes, are small compared to the expected values for spacecraft lifetime from Figure 15. Values for reentry, unaltered, were as much as hundreds or thousands of years, suggesting that these deorbit times are prohibitively short, representing only the end of a deorbit sequence.

Using the maximum lifetime numbers, specific details can be found regarding the corresponding altitudes of the CubeSat configurations. The initial scenario involves each CubeSat with a 25 m^2 sail. Figure 31 shows the lifetimes of the spacecraft based on the initial altitude. For these cases, spacecraft are assumed to have a constant mass and frontal area throughout the integration of Equation 4.

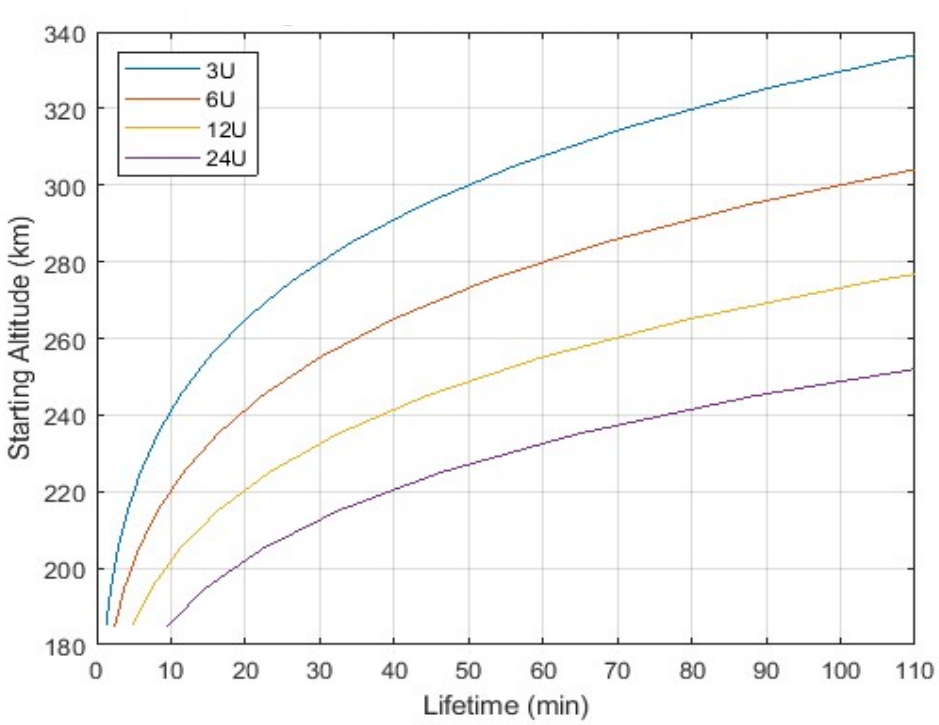

Figure 31. Orbital Lifetimes for CubeSats with a 25 m^2 Drag Sail

The next step is to compare Figures 30 and 31. The maximum lifetime values on the y-axis of Figure 30 can be compared to the x-axis values in Figure 31 to find the maximum starting altitude for a targeted reentry scenario. Table 5 shows the maximum altitudes that correspond to the safe reentry corridors in Table 4 to the nearest kilometer. The data shows that larger spacecraft require longer reentry times and have lower acceptable target reentry altitudes. For reference, the International Space Station orbits at about 400 km. With all values in Table 5 observed in the 200 km to 350 km range, the targeted reentry altitudes are consistent with the altitudes in which a spacecraft mission may occur. Using drag sails for targeted reentry may be feasible for spacecraft without manipulating the initial conditions. For spacecraft above these altitudes, reentry targeting cannot be achieved passively from its initial altitude. Alternatively, the spacecraft can begin its deorbit process without targeting and initiate a sail deployment sequence when it reaches the necessary altitude.

Table 5. Maximum Altitude for CubeSat Sizes/Reentry Corridors with Drag Sail, in km

Reentry Corridor	**15°**	**30°**	**45°**	**60°**	**90°**
3U	259	285	302	314	332
6U	236	260	275	286	302
12U	216	237	250	261	275
24U	198	216	228	237	251

For comparison, the process was repeated using CubeSats without a drag sail. The resulting data is shown in Figure 32. The initial altitudes are significantly lower than the drag sail iteration for the scenario. No scenario allows for a targeted reentry at an altitude above 145 km. In this investigation, based on literature, spacecraft are considered deorbited at 180 km, a point at which no orbit can be sustained for any relevant period of time [17]. Although the timeframes show that the lifetimes are still one to two hours, this information suggests no spacecraft may practically operate below this altitude range. As such, it is not feasible to attempt passive targeted reentry of a spacecraft without an additional deorbit accelerating device, such as a drag sail.

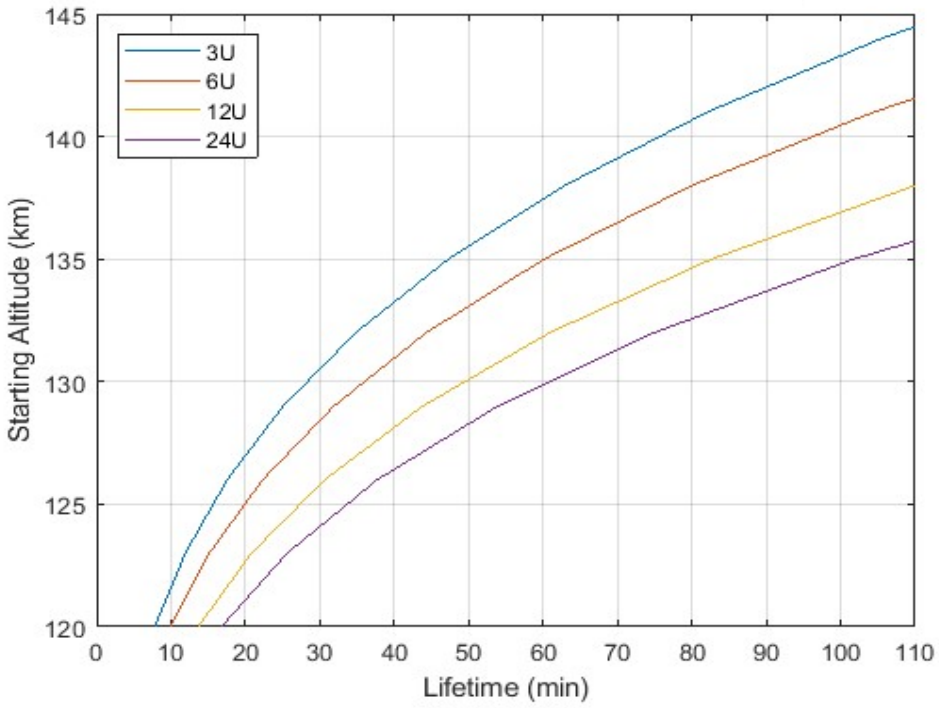

Figure 32. Orbital Lifetimes for CubeSats with no Drag Sail

Reentry Corridors Example

To thoroughly analyze the deorbit strategy, the altitude data can be factored into specific scenarios for targeting. Two situations are considered: first, a 24U CubeSat with a 90° corridor, targeting the middle of the Pacific Ocean, then a 24U CubeSat with a 45° corridor, targeting the middle of the Atlantic Ocean. Initial altitudes can be retrieved from Table 5, and other orbital elements can be selected by backtracking from the targeted location. Starting parameters are shown in Table 6. Both scenarios are propagated forward from J2000, the time constant referring to January 1, 2000, at 00:00.000 UTC.

Table 6. Initial Orbital Elements for Example Targeting Scenarios

	Starting Altitude (km)	**e**	**i (°)**	**Ω (°)**	**ω (°)**	**θ (°)**
Scenario 1	251	0	30	170	60	30
Scenario 2	228	0	30	280	60	250

Scenario 1 is first implemented into the orbit propagator. A 150°W longitude is selected as a potential location to deorbit a spacecraft in the Pacific Ocean. The latitude is arbitrary for a situation in this region because not many landmasses are situated laterally. Figure 33 shows the reentry corridor, highlighted in white, and the targeted location on a plot of the Earth's surface. It also shows the spacecraft's initial state in blue. The spacecraft completes 1.25 orbits in 107 minutes before the reentry state is reached, noted in red.

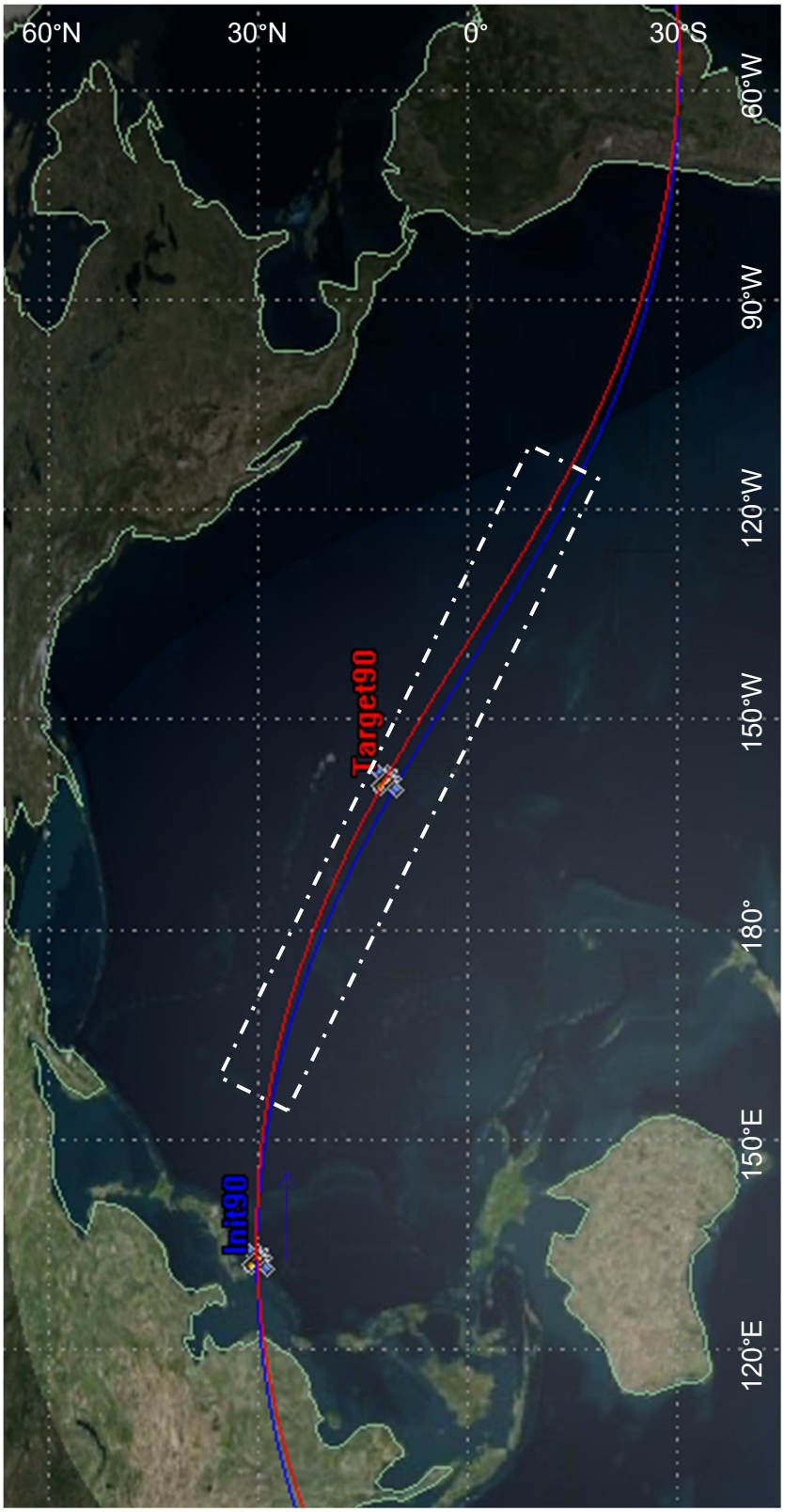

Figure 33. 90° Target Corridor for 24U CubeSat with Drag Sail [18]

Note that reentering in this area of the Earth allows for large error, potentially exceeding 90°. Other factors, such as inclination and location of the ascending node, may affect the viability of the spacecraft deorbit. Note the position of the target location near the descending node in Figure 33. The position of the node allows for more freedom in this area since South America is further east than North America. Had the target been situated on the ascending node, the locations of both North America and the South Pacific islands may have limited the acceptable reentry corridor. The proximity to landmasses is a mission-specific concern and needs to be addressed for each scenario. The actions for pursuing a safer reentry are primarily the same in each case, lowering the altitude and shortening the reentry corridor.

While the Pacific Ocean is the ideal option for safe deorbit, there are other options, with the next largest being the Atlantic Ocean in Scenario 2. To reenter in this ocean, the longitude of the reentry corridor is decreased from 90° to 45°, while still using a 24U CubeSat. The change of longitude results in a decrease of 23 km in initial altitude. All other orbital elements remain the same, except for the right ascension of the ascending node, which is increased by 110° for the new target location of 30°W. To ensure that the target reaches its intended location, the true anomaly is set to 250°. The ground track for Scenario 2 can be seen in Figure 34. Noting its starting location in yellow, the scenario takes 0.6 orbits in 54 minutes to reach its reentry location, with the final state in green.

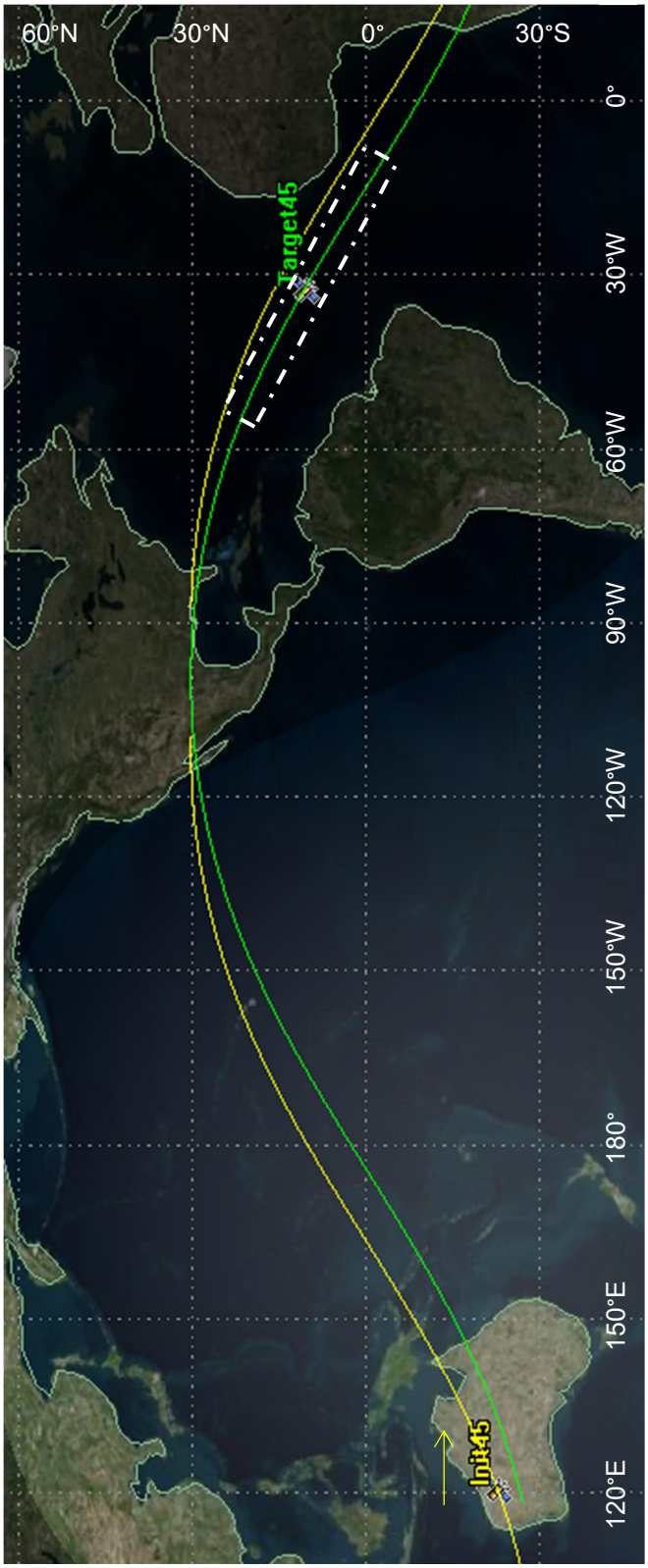

Figure 34. 45° Target Corridor for 24U CubeSat with Drag Sail [18]

In analyzing Figure 34, similar topics as Figure 33 can be noted. Safe reentry in the Atlantic Ocean is more heavily subject to the location of the nodes than targeting a location in the Pacific Ocean. Scenario 2 involves the reentry corridor near the descending node. In this situation, the corridor may be safely increased to 60°. However, had the orbit been near-equatorial or the nodes switched, the longitude corridor value would have to be significantly decreased due to the locations of nearby landmasses. Switching of the nodes in an equivalent situation would have required the safe reentry corridor to drop below 30°.

The primary concern with making an overarching analysis of the passive reentry problem is that every mission has unique problems and solutions. Scenarios 1 and 2 represent specific cases in which passive reentry can be applied, although they are idealized to investigate particular solutions. For example, in real-life missions, the initial conditions for orbital elements are likely to be fixed. The only variable that could be modified is the true anomaly, which is continuously changing. However, the procedure for analyzing the targeting process should remain the same. The preceding analysis explores the mission-specific needs and safety precautions necessary to ensure mission success.

Large Spacecraft

For additional analysis, the concept of applying drag sails to larger spacecraft is to be further investigated. ENVISAT, ICESAT, and Iridium were previously used examples of spacecraft types that inhabit low-Earth orbit and could benefit from passive reentry procedures. The analysis is similar to that of the CubeSats with the application of Equation 4; however, the initial conditions are modified. Refer back to Table 3 for the relevant data.

Four scenarios are considered: one for each of the three satellites in Table 3 with 25 m^2 sails, then a scenario in which the spacecraft's sails are scaled to meet the 25-year lifetime requirement, 566 m^2 for ENVISAT and 45 m^2 for Iridium. The analysis in Table 3 showed that for ENVISAT and Iridium, a 25 m^2 sail was not sufficient to meet the 25-year deorbit threshold. For ICESAT, the 25-year threshold was met in a sail-less configuration. The difference of ICESAT is the significantly lower starting altitude that results in lower deorbit times. For the fourth scenario, given that the other two spacecraft are both in the 770-780 km altitude range, the area-to-mass ratio that drives deorbit remains constant for a 25-year deorbit. Given the consistency, both Iridium and ENVISAT can be considered in one scenario. Figure 35 shows the starting altitude vs. lifetime for each of the four scenarios.

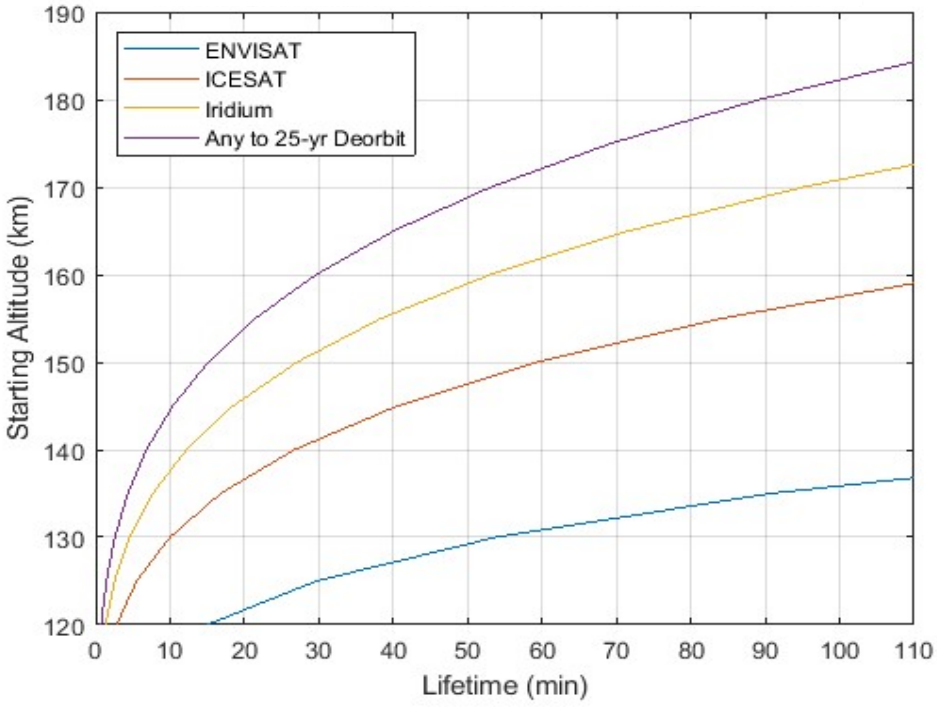

Figure 35. Orbital Lifetimes for Large Satellite Scenarios, with Drag Sails

Note, the range of altitudes is much more comparable to the sail-less CubeSat situations. At the lower lifetimes, the altitudes are not viable to begin a reentry sequence. For the 25-year scenario, altitudes exceed 180 km at higher reentry ranges and become more reasonable as a starting location. The result makes logical sense given that for the larger spacecraft with 25 m^2 sails, each example still maintained area-to-mass ratios similar to those of sail-less CubeSats, according to Table 2.

From this result, decisions on sail usage become a matter of trade-offs. One could conceivably increase the sail size even more for an expedited reentry, but the pace would come at the cost of extra weight. Depending on the parameters, it might not be worth it to significantly accelerate the deorbit to meet the passive targeting restrictions. The ideal solution comes down to the goals of the mission.

DISCUSSION

Having shown the process and outcomes of implementing passive reentry, this final section will consider the data and discuss practical considerations and recommendations for pursuing a passive spacecraft disposal method with drag sails. The discussion primarily concerns the realistic application of the process and draws conclusions for the assumptions and parameters. The main points involve comparing the two processes for orbital lifetime estimates: Euler approximation and numerical integration, then realistically applying the targeted reentry steps to real-world scenarios.

Applications of Drag Sail Deorbit

When comparing the two methods, it is apparent that the differences in the lifetime estimates do not warrant the extra computational cost of performing complete numerical integration in most cases. The numerical integration is beneficial because spacecraft location can be referenced at any time, making it the ideal method for gathering information throughout a propagation. When estimating the magnitude of the orbit lifetime, numerical integration with comprehensive perturbation analysis does not significantly affect the analysis. With this information, drag can reasonably be the only perturbation considered when analyzing lifetime data. The result of including solar radiation pressure was that the lifetime could be decreased at sufficiently high area-to-mass ratios. The limitation of the assumption is that for a 24U CubeSat, the decrease in the flight time was only a few weeks for a propagation that may last decades. A 24U CubeSat with a 25 m^2 drag sail has a significant area-

to-mass ratio initially, suggesting further increases in sail size may be unreasonable for a realistic spacecraft configuration.

Because of the minimal effect of SRP on changing a spacecraft's trajectory, it may be more practical to treat it as negligible. For targeting and tracking purposes, it would mean using a transparent sail instead of a reflective solar sail. Driving the solar radiation pressure coefficient to zero would imply that the SRP force can be considered zero and neglected. The assumption is limited to the orbits studied up to 1000 km, with spacecraft at higher altitudes more significantly perturbed by SRP than drag forces. Pursuing transparent sails may mean further evaluation of materials used in construction is required; however, this should not be considered a limitation at the current time.

Moreover, it was shown that leveraging drag is an effective way to induce the deorbit of a spacecraft in the considered range. Nearly all scenarios showed promise in using a reasonably sized sail to meet the 25-year NASA requirements. The cases that didn't meet the boundaries of current technology cannot be ruled out completely, given that as technology advances, the limits may be met as well. The one noteworthy issue is that there is a difference in forces exerted on a sail between those expected from a solar sail and those from a drag sail, particularly at low altitudes. The increase in stress may require the construction to be bolstered, likely increasing mass requirements. However, this conclusion would require further analysis, given that there is no inherent reason why current technology could not stand up to the forces accompanying high velocities with high drag. Purely from the standpoint of inducing deorbit in sufficient time using drag sails, this investigation supports the effectiveness of pursuing drag sails as a spacecraft disposal method.

However, effective disposal from a performance standpoint is inadequate if the program is not cost-effective. It was noted that current methods require the use of propulsion to induce atmospheric reentry. Currently, the cost to deliver a kilogram of mass to low-Earth orbit is about $10,000. To create a valid reason to pursue drag sails, they must be more mass-efficient in delivery than to carry extra fuel for the sole purpose of expelling it in reentry. The cost metric also overwhelmingly points towards drag sails as a viable option for spacecraft disposal. Using Figure 17, for a 24U CubeSat from 1000 km, the mass savings was one kilogram, cutting $10,000 off a simple CubeSat mission. This saving is the absolute minimum for this size spacecraft. The same comparison from 800 km, due to the exponential nature of atmospheric drag, saves closer to $20,000. These numbers only become more exaggerated as the spacecraft become larger. For ENVISAT, the largest specific spacecraft studied, the mass required for a sail and propellant is 68 kg and 580 kg, respectively, according to Table 3. This decrease results in a cost savings of $5.12 million just by adapting the deorbit process for drag sails. Space travel is an expensive endeavor, but cost savings of such magnitude are significant incentives to pursue innovative methods when planning a satellite mission.

From an application standpoint, the drag sail could simply be a box attached to the spacecraft from initial deployment. When the spacecraft reaches the end of its mission and the time comes to commence disposal operations, the sail could then be deployed and begin the removal process. The additional cost savings on fuel could be used to extend the mission's life, or it could merely result in cost savings upfront. Regardless of how the operator decides to perform the mission, a drag sail could result in substantial cost savings for a mission and simplify the end-of-life operations by removing a large portion of the planning and monitoring required to dispose of the spacecraft manually.

Applications of Targeted Reentry

The conclusion that a drag sail can successfully deorbit a spacecraft is incomplete without assurance that the process can be safely applied. Safety considerations require the successful use of a variety of targeting procedure. It was shown that, at certain altitudes, it is reasonable to apply passive deorbiting techniques to a spacecraft using drag sails. A significant amount of mission variability needs to be addressed; however, applying the techniques based on the intended reentry corridor was a functional concept. In the scenarios addressed, specific areas on Earth are safely and effectively targeted.

As far as practicality, there is still more work to treat this reentry method as sufficiently usable. While it proved to be an option up to 350 km, many missions would benefit from passive reentry as high as 1000 km or more. The reentry target error would be too large to be safe at those altitudes, spanning several orbits and reentering in a random location. However, a mission could conceivably involve starting reentry arbitrarily, then pursuing its passive targeting as the spacecraft reaches the altitudes shown in the study. The process would require a method of easily deploying and retracting the sail because if the sail is retracted near the targeting altitudes, it could effectively reset and then begin targeted reentry safely. Additional analysis would be required to confirm the feasibility of the method for targeted reentry above 350 km.

Consider a scenario in which a spacecraft's mission altitude is around 800 km, well above the range that could be targeted from the beginning. The spacecraft carried aboard a drag sail for end-of-life disposal. At the end of its mission life, the drag sail is deployed to begin the deorbit process. The altitude decreases over time until the spacecraft reaches around 200 km, depending on its mass and intended reentry corridor, then the sail retracts in order for the spacecraft to be reoriented along its trajectory. From there, the spacecraft could redeploy its sail

to complete the deorbit once the orbit reaches a state in which the reentry sequence could be initiated safely. The process would complete the disposal, still in the allotted time, without removing the passive nature of the deorbit. The additional steps would require further mission planning, but the disposal could be completed efficiently without sacrificing the safety of those on the ground.

This targeted reentry process could feasibly work; however, it is not likely to be the most efficient method. It is an effective initial concept but may require significant additional work to fully finalize the passive reentry process. It does show that a drag sail spacecraft can be safely deorbited in the short-term without significant advances in technology. Considering this and the conclusion that drag sails can increase the efficiency of the disposal process, it is apparent that the concept is worthy of additional high-fidelity analysis and real-world testing. The primary consideration of the method is the trade-off between control and simplicity. Passive control shows promise in the cost category, with the potential for considerable savings, but may be insufficient to meet the mission's needs without further investigation.

CONCLUSION

In concluding this work, a few topics will be discussed. First, the work is summarized, and overarching conclusions restated. Second, recommendations for further analysis of this work are discussed. The concept of drag sails is relatively new but shows significant potential moving forward. With additional analysis, it may become an effective and efficient way to decrease the amount of debris in low-Earth orbit in the near future. Effectively addressing this issue can extend the use of space as a medium for human development projects deep into the future. This drag sail operation analysis suggests that the concept can successfully meet all mission requirements and is a strong baseline for further implementing the technology to address future mission needs.

Summary

This work largely consisted of two topics relating to spacecraft disposal using drag sails: orbital lifetime of spacecraft with drag sail sizing and applying a sail to perform passive reentry targeting. Within the context of orbital lifetime, two methods were performed to verify the data. Following this, conclusions were made about the real-life application of the process to spacecraft missions.

Initially, the sails were assumed to be only affected by atmospheric drag. Solving the lifetime involved integrating the results of certain equations until a predetermined final state was reached. The method intended to complete a big-picture analysis of the lifetimes for a range of spacecraft initial conditions. A comparison of this process to the current methods of

targeted propulsive reentry was made. The conclusion was made that it is more efficient, from a mass standpoint, to deorbit using drag sails instead of the propellant.

Building upon the initial method, a similar analysis was performed using numerical integration. The in-depth look considered a wider range of perturbations, factoring in solar radiation pressure and J_2. Numerical integration was different in that it was not time-efficient for considering a wide range of initial conditions, instead being able to look at a broader range of time-specific parameters throughout the spacecraft's lifetime. Instead of general trends, it provided a way to look at an in-depth propagation of the orbit. From comparing the two methods, the lifetime predictions came out to the same deorbit times. Moreover, it was concluded that drag could be isolated in the propagations, as solar radiation pressure and J_2 proved to have a negligible effect on the spacecraft's lifetime over the long term.

With lifetime addressed, the final consideration was targeting the reentry into Earth's atmosphere with the available technology. In this study, a 25 m^2 fixed drag sail was considered as the exclusive method to deorbit a spacecraft. With a fixed sail as the only option, the targeting method was considered purely passive and based only on the initial conditions of the propagation to provide the targeting needs. With proper mission planning, it was shown that the passive method is sufficient to target a reentry point along a specified corridor. The deorbit corridor is chosen based on a specific mission, and the maximum altitude to meet the requirement was found based on the initial spacecraft specifications. From there, spacecraft trajectories were propagated to show how a specific location on Earth could be targeted. It was shown that the altitudes required for targeted reentry of CubeSats were consistent with realistic mission orbits; however, with larger spacecraft, the altitudes necessary were lower than what could reasonably

be expected. As such, further analysis would be required as far as the mission design and application of a drag sail to deorbit larger spacecraft.

Future Work

For building up the concept of drag sail reentry for operational use, additional work would mainly consist of refining the technology and sail construction associated with the real-life product, as well as higher fidelity analysis of the deorbit strategy. For the drag sail, an analysis of structures and layout would be essential to optimize strength with mass for best performance. It would need to be light enough to maintain the cost efficiency while maintaining enough strength to withstand the drag forces at the low end of the altitude range. Additionally, construction must be done in a way to ensure that stability criteria are met. It is vital to a project like this that a wide array of stability concepts are analyzed. Due to the system's inherent instability, no project of this type can be progressed without first comprehensively analyzing the stability of the system.

Targeted reentry could be progressed naturally by addressing the concept of drag sail variation throughout the orbit. Instead of being fixed, the sail area could be varied consistently to perform corrections over the course of the entire orbit. This concept would create a more cohesive end-of-life operation than the one proposed. The D3 project is a good baseline for this concept, and it may be worth pursuing concurrently with other aspects of drag sail implementation to prepare for the required testing. A variable drag sail deorbit would remove the entirely passive nature of this work while still deorbiting a spacecraft exclusively due to natural perturbations.

A project like this may show promise in the analytical investigation; however, significant flight testing is required to get the concept to an operational state. Tests on the ground and in space could begin to show issues that may not have been addressed on a computer. Building the product is of vital importance and is a natural next step in the process. Some examples have been built already, but the flight testing that has been performed is minimal beyond simply confirming the technology. Moving forward, a wide range of flight test missions are recommended to take the concept and validate the efficiency of the spacecraft disposal.

REFERENCES

[1] Johnson, N. L., "Orbital Debris: The Growing Threat to Space Operations," 33rd Annual Guidance and Control Conference, AAS 10-011, February 2010, pp. 7-8.

[2] Yost, B., "State of the Art Small Spacecraft Technology," NASA/TP-2018-220027, December 2018.

[3] Ansdell, M., "Active Space Debris Removal: Needs, Implications, and Recommendations for Today's Geopolitical Environment," Journal of Public and International Affairs, Vol. 21, No. 1, 2010, pp. 7-22.

[4] Stohlman, O. R., Schenk, M., Lappas, V., "Development of the DeOrbitSail Flight Model," SciTech Forum, AIAA, January 2014.

[5] Taylor, B., Underwood, A., Viquerat, S., et al., "Flight Results of the InflateSail Spacecraft and Future Applications of Dragsails," 32nd Annual Conference on Small Satellites, AIAA/USU, August 2018.

[6] Mogi, T., Kuwahara, T., Uto, H., "Structural Design of De-orbit Mechanism Demonstration CubeSat FREEDOM," JSASS Aerospace Tech, Vol. 14, No. 30, 2016, pp. 61-68.

[7] Lappas, V., Pellegrino, S., Straubel, M., et al., "DeOrbitSail: De-orbiting of Satellites using Solar Sails," 2nd International Conference on Space Technology, IEEE, September 2011.

[8] Hedin, A. E., "High Altitude Atmosphere Modeling," NASA TM-100707, October 1988.

[9] McInnes, C. R., "Solar Sailing: Technology, Dynamics, and Mission Applications," 1st ed., Springer-Praxis, 2004, pp. 2.

[10] Garner, C., Leipold, M., "Developments and Activities in Solar Sail Propulsion," 36th Joint Propulsion Conference and Exhibit, AIAA/ASME/SAE/ASEE, July 2000.

[11] Mori, O., Sawada, H., Funase, R., et al., "First Solar Power Demonstration by IKAROS," JSASS Aerospace Tech, Vol. 8, No. 27, 2010, pp. 25-31.

[12] Curtis, H. D., "Orbital Mechanics for Engineering Students," 3rd ed., Elsevier, 2014, pp. 652-720.

[13] Guglielmo, D., Omar, S., and Bevilacqua, "Drag Deorbit Device: A New Standard Reentry Actuator for CubeSats," Journal of Spacecraft and Rockets, Vol. 56, No. 1, September 2018.

[14] Black, A. and Spencer, D., "DragSail Systems for Satellite Deorbit and Targeted Reentry," 1st International Orbital Debris Conference, December 2019.

[15] Wilcutt, T. W., "Process for Limiting Orbital Debris," NASA-STD-8719, August 2007.

[16] Mostaza Prieto, D., Graziano, B. P., Roberts, P., "Spacecraft Drag Modelling," Progress in Aerospace Sciences, 64, 56-65, January 2014.

[17] Kennewell, J., "Satellite Orbital Decay Calculations," Australian Space Weather Agency, IPS Radio and Space Services, 1999.

[18] STK, Satellite Tool Kit, Software Package, Ver. 11.7.1, Analytical Graphics Inc, Exton, PA, 2018.

[19] Wertz, J.R., "Spacecraft Attitude Determination and Control," 1978 ed., Kluwer, Dordrecht, 1978, pp. 820.

[20] Jursa, A., "Handbook of Geophysics and the Space Environment," U.S. Air Force Geophysics Lab., AFGL-TR-85-0315, Hanscom AFB, MA, December 1985.

[21] Lewis, B., "Complete 1976 Standard Atmosphere," Matlab Central File Exchange, University of Colorado, 2007.

[22] Hull, S., "End of Mission Considerations," NASA NTRS, January 2013, pp. 4.

[23] Hill, P. G., Peterson, C. R., "Mechanics and Thermodynamics of Propulsion," 2nd ed., Addison-Wesley, 1992, pp. 573-577.

[24] Georgevic, R. M., "Mathematical Model of the Solar Radiation Force and Torques Acting on the Components of a Spacecraft," NASA TM 33-494, October 1971.

[25] Xu, G., Xu, J., "On Orbital Disturbing Effects of Solar Radiation," Royal Astronomical Society, MNRAS 432, 584-588, April 2013.

[26] Long, A. C., Spencer, D. A., "Stability of a Deployable Drag Device for Small Satellite DeOrbit," SPACE Forum, AIAA/AAS, September 2016.

[27] Christ, R., "Computation of Sub-Satellite Points from Orbital Elements," NASA TN D-2771, July 1965.

[28] "Implications of Using the World Geodetic System 1984 (WGS84)," World Meteorological Organization, Commission for Basic Systems, 6th Session, April 2011.

[29] "CubeSat 101: Basic Concepts and Processes for First-Time CubeSat Developers," NASA CubeSat Launch Initiative, California Polytechnic State University, San Luis Obispo, CubeSat Systems Engineer Lab, October 2017.

[30] "eo: Sharing Earth Observation Resources," eoportal, online database, August 2020.

[31] Heiligers, J., Diedrich, B., Derbes, B., and McInnes, C. R., “Sunjammer: Preliminary End-to-End Mission Design,” Astrodynamics Specialist Conference, AIAA/AAS, August 2014.